https://ntrs.nasa.gov/search.jsp?R=20180003450 2019-09-26T19:28:07+00:00Z

The impact of SST-forced and unforced teleconnections on 2015/16 El Niño winter precipitation over the western United States

Young-Kwon Lim[1,2], Siegfried D. Schubert[1,3], Yehui Chang[1,4],
Andrea M. Molod[1], and Steven Pawson[1]

[1]Global Modeling and Assimilation Office, NASA GSFC, Greenbelt, MD

[2]Goddard Earth Sciences Technology and Research, I. M. Systems Group, Greenbelt, MD

[3]Science Systems and Applications Inc., Lanham, MD

[4]Goddard Earth Sciences Technology and Research, Morgan State University, MD

Corresponding Author: Young-Kwon Lim
(Young-Kwon.Lim@nasa.gov, 1-301-614-6906)

For Submission (Revised version) to Journal of Climate

April 16, 2018

Abstract

The factors impacting western U.S. winter precipitation during the 2015/16 El Niño are investigated using the Modern-Era Retrospective analysis for Research and Applications version 2 (MERRA-2) data, and simulations with the Goddard Earth Observing System version 5 (GEOS-5) atmospheric general circulation model forced with specified sea surface temperatures (SSTs).

Results reveal that the simulated response to the tropical Pacific SST associated with the 2015/16 El Niño was to produce wetter than normal conditions over much of the west coast including California – a result at odds with the negative precipitation anomalies observed over much of the Southwestern U.S. It is shown that two factors acted to partly counter the canonical ENSO response in that region. First, a potentially predictable but modest response to the unusually strong and persistent warm SST in the northeastern Pacific decreased precipitation in the Southwestern U.S. by increasing sea level pressure, driving anticyclonic circulation and atmospheric descent, and reducing moisture transport into that region. Second, large-scale unforced (by SST) components of atmospheric variability (consisting of the leading modes of unpredictable intra-ensemble variability) resembling the positive phase of the North Atlantic Oscillation and Arctic Oscillation are found to be an important contributor to the drying over the western U.S. While a statistical reconstruction of the precipitation from our simulations that account for internal atmospheric variability does much to close the gap between the ensemble mean and observed precipitation in the Southwestern U.S., some differences remain, indicating that model error is also playing a role.

1. Introduction

The El Niño that occurred in 2015/16 ranks as one of the strongest events in the last 6 decades (Bell et al. 2016; Huang et al. 2016; L'Heureux et al. 2016; Lim et al. 2017). Strong El Niños have historically produced wet conditions over the Southwestern United States (US) (Ropelewski and Halpert 1986; Cayan et al. 1999; Larkin and Harrison 2005; Lau et al. 2008; Hoell et al. 2016; Jong et al. 2016) and as such, the 2015/16 event was expected to ameliorate the long-lasting drought over California. That fact that this did not occur came as a surprise to much of the climate community and ran counter to the numerous predictions for ENSO SST-forced wet conditions over the Southwestern US that winter (e.g. http://www.cpc.ncep.noaa.gov/products/NMME/archive/2015110800/current/usprate_Seas1.html ; http://www.wrcc.dri.edu/enso/WRCC_ElNino_092015.pdf). The focus of this paper is to examine the reasons why the 2015/16 strong El Niño apparently failed to produce the expected wet conditions over the Southwest (especially in Southern California and Arizona).

We consider a number of factors that might have contributed to the observed negative precipitation anomalies over the Southwestern US during the winter of 2015/16. These include a possible change in the character of ENSO, a response to the SST associated with a vast pool of warm water off the North American west coast, and unforced internal atmospheric variability.

There is now considerable evidence that the character of ENSO is not constant but in fact has different “flavors” (Ashok et al. 2007; Kao and Yu 2009; Kug et al. 2009): an eastern Pacific (EP) El Niño and a central Pacific (CP) El Niño, differentiated by the location of the maximum warming region over the equatorial Pacific (in the Niño 3 (150°W–90°W) or Niño 3.4 region (170°W–120°W) during EP El Niños, and the Niño 4 region (160°E–150°W) during CP El Niños). In addition, several studies suggest that the frequency of extreme El Niño events are projected to increase under global warming (e.g., Cai et al. 2014), along with an increase in the ratio of CP to EP El Niño events (Yeh et al. 2009; Kim and Yu 2012). While some ENSO events are clearly distinguished as either CP or EP, there are also many events that commingle them (Capotondi et al. 2015). For example, the 2015/16 El Niño was characterized by the maximum SST anomaly occurring in the Niño 3.4 region (Bell et al. 2016; L'Heureux et al. 2016). The warming, however, extended to west of the dateline, while the SST anomalies in the far EP were rather weak. Lim et al. (2017) concluded that the 2015/16 El Niño event had characteristics of both central and eastern equatorial Pacific warming, whereas the 1997/98 and 1982/83 events were strong EP type El Niño events. There is evidence that such a difference in the SST anomalies could have led to a different response over North America including the Western US (e.g., Washington, Oregon, California, and Arizona) (Hoerling et al. 1997; Trenberth et al. 1998; Barsugli and Sardeshmukh 2002; Yu et al. 2012; Yu and Zou 2013). For example, earlier studies suggested that both the Pacific North American (PNA) and the Tropical Northern Hemisphere (TNH) (Mo and Livezey 1986; Barnston et al. 1991) teleconnection patterns spanning the extra-tropical Pacific and North America are sensitive to the type of El Niño (Mo, 2010; Yu et al. 2012): the positive phase of the PNA tends to be more active when the El Niño has CP warming, while the negative phase of the TNH is more active in events with primarily EP warming. It is noteworthy that the PNA response appears to also be influenced by the phase of Quasi-Biennial Oscillation, so it may not always be in a strong positive phase during El Niño events (Garfinkel and Hartmann 2008).

The role of a so-called warm water blob (WWB), a vast pool of warm water off the North American coast, has received considerable attention since it was first observed in 2013 (Bond et al. 2015). Development of the WWB in 2013 was not related to other recognized patterns of ocean variability such as those associated with ENSO or the Pacific Decadal Oscillation (PDO) (Mantua et al. 1997; Lorenzo and Mantua 2016). There is evidence that the WWB negatively affected marine life over the Pacific coast. It was reported that marine ecosystems suffered and the food web was disrupted by the abnormally warm, less nutrient-rich Pacific Ocean water (e.g., Opar 2015; Whitney 2015). As to the impact on weather/climate, earlier studies concluded that the hot and dry conditions over the Western US might be tied to the WWB. For example, Bond et al. (2015) found a lagged-relationship between the WWB and surface air temperature in Washington State. Hu et al. (2017) suggested that the persistent atmospheric anomalies in the northeastern Pacific in 2015 could be explained by both the impact of the WWB and the strong 2015/16 El Niño. The WWB also appears to be associated with radiative fluxes and precipitation/evaporation above the northeastern Pacific Ocean (Blunden and Arndt 2016). However, the extent to which the WWB is responsible for the Western US drought and especially the unexpected dry conditions over California during 2015 is unclear.

Internal modes of atmospheric variability (unforced by SST) are known to impact climate variability over the US (Hoerling and Kumar 1997; Thompson and Wallace 1998; Kamae et al. 2016), including Southwestern US precipitation (Seager et al. 2015). There is in particular evidence that the North Atlantic Oscillation (NAO) and the Arctic Oscillation (AO), while having substantial impact on variability over the Eastern US, also play a role in modulating the Southwestern US climate (McAfee and Russell 2008; Myoung et al. 2015). The PNA is another mode of variability that is understood to be primarily internal to the atmosphere. For example, Simmons et al. (1983), Straus and Shukla (2002), Yu (2007), and Schubert and Lim (2013) found that the PNA can be generated with little direct forcing from ENSO though, as mentioned earlier, there is evidence that ENSO can act to modulate the PNA. Regarding the ENSO impact on the PNA, the positive phase of the PNA tends to be more active during CP warming events. However, the main geopotential height and cyclonic circulation anomalies over the extra-tropical Pacific associated with the positive phase of the PNA tend to be located far from the Western US coast. Thus, the moist southerly (and southwesterly) flow in the eastern side of this cyclonic circulation anomaly does not efficiently supply moisture to the California region, and it is not very influential in driving wet conditions over the Southwestern US during El Niño (Leathers et al. 1991; Woodhouse 2003; Ge et al. 2009; Yu et al. 2012).

We address the extent to which the above factors impacted Southwestern U.S. winter precipitation during the 2015/16 El Niño using the Modern-Era Retrospective analysis for Research and Applications version 2 (MERRA-2) (Gelaro et al. 2017) data, and various simulations with the NASA Goddard Earth Observing System version 5 (GEOS-5) atmospheric GCM (AGCM) (Molod et al. 2015) with specified SST. The paper is organized as follows. Section 2 introduces the reanalysis data, models, and experimental design. The North American winter climate during the 2015/16 El Niño event is described and compared with those of other past strong El Niño events (1982/83 and 1997/98) in Section 3. Section 4 describes the results obtained from the AGCM simulations, including an assessment of the role of the WWB during the 2015/16 ENSO event. The predictability and contribution of unforced atmospheric variability to the Southwestern US precipitation is addressed in Section 5. Section 6 discusses the results in previous sections and the sensitivity of the precipitation response to the character of equatorial Pacific SST, and addresses some remaining issues.

2. Data and Model Experiments

2.1. Reanalysis and Observations

The primary atmospheric reanalysis data for this study is MERRA-2 (Gelaro et al. 2017). MERRA-2, developed by NASA Goddard Space Flight Center (GSFC) / Global Modeling and Assimilation Office (GMAO), is an updated version of MERRA (Rienecker et al. 2011) with an improvement of the model's physical parameterizations including moist process[1], turbulence, land and ocean surface, and gravity wave drag (Bosilovich et al. 2015; Molod et al. 2015; Gelaro et al. 2017). The key variables used here consist of 2-meter air temperature, precipitation, sea level pressure, 850mb wind and specific humidity, and geopotential height at 500 and 250mb (GMAO 2015a,b,c). The horizontal resolution of the MERRA-2 data is 0.625° longitude ×0.5° latitude. The observed SST used for analysis and AGCM experiments consist of the NOAA Optimal Interpolation Sea Surface Temperature (OISST) data (Reynolds et al. 2007) and Operational Sea Surface Temperature and Sea Ice Analysis (OSTIA) data (Donlon et al. 2011).

2.2 NASA GEOS-5 model

We use the NASA GEOS-5 AGCM for the model experiments[2] performed for this study. The model is run with 72 hybrid sigma-pressure vertical levels, extending to 0.01hPa, and 1.25° latitude/longitude horizontal grid spacing. The convection scheme is a modified version of the Relaxed Arakawa Schubert (RAS) scheme of Moorthi and Suarez (1992). It includes a stochastic Tokioka trigger function (Tokioka et al. 1988; Bacmeister and Stephens 2011) that governs the lower limits on the allowable entrainment plumes (Bacmeister and Stephens 2011; Lim et al. 2015; Molod et al. 2015). The model has the option for a standard single-moment microphysics (Bacmeister et al. 2006) or a two-moment cloud microphysics (Barahona et al. 2014) embedded

[1] The changes include an increased re-evaporation of frozen precipitation and cloud condensate, resolution-aware parameters, and a Tokioka-type trigger on deep convection as part of the Relaxed Arakawa-Schubert (Moorthi and Suarez 1992) convective scheme.
[2] The internal designation of the AGCM version used here is GEOS-5 Heracles 4.3.

within the RAS convective parameterization, and the simulations described here used the single moment option. The model also includes the catchment land surface model developed by Koster et al. (2000). Further details about the GEOS-5 AGCM can be found in Rienecker et al. (2008) and Molod et al. (2015).

2.3 Experimental design

We carried out a number of AGCM experiments distinguished by having different prescribed SST boundary conditions. The full list of experiments is presented in Table 1. Our control experiment (Exp CTL) has the observed SST everywhere, so it includes the impact of both the tropical 2015/16 El Niño SST and those associated with the WWB. Another experiment, Exp NW (here NW stands for "no WWB"), is forced by the same SST as Exp CTL everywhere except over the northeastern Pacific region, where the SST associated with the WWB are removed. In order to do that, we compute the component of the SST in that region forced by the 2015/16 El Niño itself. To estimate that contribution, we regress the observed SST anomaly for the period 1951–2014, (with the global mean trend removed) onto the Niño 3.4 index, and then scale the regressed SST anomalies based on the magnitude of the 2015/16 Niño 3.4 index. This procedure for estimating the SST associated with the 2015/16 El Niño is conducted separately for each month from June through February, which covers the El Niño growth to maturity. These estimates, which now include only the SST anomalies associated with the 2015/16 El Niño, are then prescribed over the northeastern Pacific in the Exp NW. Figure 1 outlines the SST domains for each experiment. The ensemble members are distinguished by having different atmospheric/land initial conditions taken from MERRA-2 during the 50-day period June 01 through July 20, 2015. We also conducted climatological SST–forced runs (Exp

CLIM: no El Niño and WWB effect) to compare them with those from Exp NW and Exp CTL. For these runs, the SSTs are prescribed to be climatological (SST are averaged over the period 1980-2015) everywhere with the atmosphere/land initial conditions taken from MERRA-2 for the year 2015/16. Thus, the only difference between Exp NW, Exp CTL, and Exp CLIM runs is the SST distribution prescribed in the model. The integrations are approximately nine months in length, ending on March 1 of the following year.

While the primary focus in carrying out the above experiments was on understanding the role of the WWB and internal atmospheric variability in impacting the El Niño response, we have carried out a number of additional sensitivity experiments to help clarify and confirm aspects of those runs. In particular, auxiliary experiments were done that examine the sensitivity of the response to the character of equatorial Pacific SST and to the overall strength of the El Niño. To address the sensitivity to the character of the equatorial SST, we carried out simulations with A) observed 2015/16 SST prescribed over the entire equatorial Pacific, B) observed 2015/16 SST over the central equatorial Pacific only (160°E–150°W, Niño 4 region), and C) the same as B) but for an SST composite of the recent CP El Niños (1987/88, 1991/92, 1994/95, 2002/23, 2004/05, and 2009/10) over the central equatorial Pacific. In each of those sets of runs, the SSTs are prescribed to climatology everywhere else. We will refer to this set of runs as Exp SC (sensitivity to character). Another set of runs examines the sensitivity of the GEOS–5 AGCM response to the strength of El Niño. Here, experiments were conducted which had A) the observed 1997/98 SST prescribed globally (another very strong El Niño), and B) the historic mean El Niño SST prescribed globally (the average of 1982/83, 1986/87, 1987/88, 1991/92, 1994/95, 1997/98, 2002/03, 2004/05, 2006/07, and 2009/10). We shall refer to this set of runs as Exp SS (sensitivity to strength).

3. Observed conditions during the 2015/16 winter

We first examine the observed atmospheric anomalies during the 2015/16 El Niño winter. Previous studies have shown that the US tends to have cold and wet conditions over the Southeastern, Eastern, and Southwestern US, and warm winters over parts of the Northern US during El Nino events (Ropelewski and Halpert 1986; Larkin and Harrison 2005; Seager et al. 2005; Lau et al. 2008). Figs. 2a,b,d,e show, for example, that during the 1982/83 and 1997/98 El Niño events the Western US and Southeastern US (Florida) experienced cold and wet winters, which is consistent with the canonical response to strong El Niño events. In contrast, the winter anomalies in 2015/16 are quite different (Figs. 2c,f), showing warmer and drier conditions over the Southwest.

Figure 3 provides some insight into the nature of the precipitation and temperature anomalies that occurred during the 2015/16 winter. Figure 3a shows that the winter was characterized by a strong negative SLP anomaly over the northeastern Pacific, with weak positive SLP anomalies across the Southwestern US and Mexico. Interestingly, this negative SLP anomaly is located somewhat to the northwest of that observed during previous strong El Niño years (figure not shown). We will come back to this point later in our discussion of the role of WWB in Section 4. The lower-tropospheric circulation and humidity in Fig. 3b show a large region of positive humidity anomalies over the tropical Pacific, associated with the El Niño. There is also a strong cyclonic circulation anomaly combined with the positive humidity anomalies along the western coast of North America. In contrast, the Southwestern US and Mexico are characterized by negative moisture anomalies, along with weak off-shore flow. Consistent with the lower tropospheric anomalies, the upper-tropospheric geopotential height anomaly distribution at 250mb (z250) consists of a large negative anomaly over the northeastern Pacific with a positive anomaly extending over the Southwestern US (Fig. 3c). The above atmospheric circulation and pressure anomaly patterns over the Southwestern US are unusual for a strong El Niño event, and require explanation if we are to understand the nature of the tendency for drying over that region, along with the wetter than normal conditions over the Northwestern US (Fig. 2f).

Figures 3d and 3e show that there was some evolution of the Pacific SST during the time period of the AGCM simulations. In particular, the WWB SST showed some weakening as the El Niño reached maturity in the winter 2015/16, although the positive SST anomalies are still dominant in the northeastern Pacific with the maximum greater than 1K. The fact that the largest warm anomalies are observed close to the North American west coast during the winter, suggests that the impact of the maturing El Niño (by forcing the negative SLP anomaly in the northeastern Pacific discussed above) was to reduce the strength of the warming in the central North Pacific (Lorenzo and Mantua 2016).

We next examine whether SST anomalies other than those in the tropical Pacific contributed to the unexpected seasonal precipitation anomalies over the Western US during the winter 2015/16. We focus in particular on isolating the role of the SST in the northeastern Pacific (the WWB) and how that compares with the forcing from SST elsewhere including the ENSO-related tropical Pacific SST.

4. Response to the WWB and 2015/16 El Niño

Here we use AGCM experiments to isolate the roles of El Niño and the northeastern Pacific WWB on the Western US climate during the 2015/16 El Niño. We simulate the response to the mature phase of the 2015/16 El Niño both with and without the WWB SST (region is defined in Figure 1). A key question is whether the response to the El Niño – related SST was unusual (in that it produced drying over the Southwest) or whether instead the response to El Niño was to produce wet conditions over the Southwestern US (as expected), but the WWB SST acted to reduce that response.

Two sets of AGCM experiments with prescribed SST were performed, as described in Section 2.3. Exp NW excludes the northeastern Pacific WWB SST, while Exp CTL is a control in which observed SST is specified globally. Figure 4 shows the z250 and precipitation anomalies produced in the control (Exp CTL) for the 2015/2016 winter. The two negative anomalies of z250 over the northeastern Pacific and the Southeastern US, and the weak positive anomalies over the Southwestern US found in the observations (Fig. 3c and contour lines in Fig. 4a) are to a large extent reproduced by the AGCM simulation (Fig. 4a (shaded)). However, a more detailed comparison with the observations (contour lines in Fig. 4a) shows that the center of the AGCM-produced negative height anomalies over the northeastern Pacific is slightly to the southeast of the observed center of anomalies. It appears that 1) this slight shift in the negative height anomalies and the associated cyclonic circulation anomalies is associated with the overestimation of the precipitation over the Southern California, Arizona, and Northwestern Mexico (weak positive rather than the observed negative anomalies; compare Figs. 4b and 2f). We also see 2) large difference in precipitation over the Eastern US. We will come back to these discrepancies over the US in section 5. In contrast, the observed positive anomalies near the coastal line of Northwestern US and the Southwestern Canada (Fig. 2f) are faithfully reproduced by the model (Fig. 4b).

The above results are unexpected in that the response to the global SST did not produce the large wet anomalies over the Southwest expected from the canonical response to tropical Pacific SST anomalies associated with a strong El Niño (compare Fig. 4b with Figs. 13a and 14a), suggesting SST anomalies in other regions may have played a role in suppressing that response. In order to address the role of the WWB we turn to Exp NW, in which the WWB SSTs in the northeast Pacific are removed. Fig. 5a shows that the precipitation anomalies for the 2015/16 winter season in that run are indeed characterized by positive anomalies over much of the Southwestern US and Northwestern Mexico. As we shall see in Section 6, this is primarily the canonical impact from the strong equatorial El Niño SST anomaly (e.g., similarity between Fig. 5a and Fig. 13a). The difference in precipitation between Exp CTL and Exp NW shown in Fig. 5b clearly demonstrates that the WWB SSTA modulates the El Niño impact by reducing precipitation over the Southwestern US and part of Mexico.

Figs. 5c,d summarize the results of the two sets of experiments over the SW (110°–123°W, 25°–37°N) and NW (120°–130°W, 38°–55°N) regions in terms of a Box and Whisker plots. The figure highlights the modest drying impact of the WWB over the SW region and wet condition over the NW. The results (in particular the ensemble spread encompassed by the whiskers) also leave open the possibility that internal variability might have played a role in acting to further counteract the canonical El Nino response in the SW region (we will address that in the next section). It is, however, also clear that even after accounting for internal variability, the model results cannot fully account for the observed anomaly which lies outside the model spread in the SW (Fig. 5c) (thought that is not the case over the NW (Fig. 5d)). We will come back to a discussion of the role of model error in Section 6.

The lower-tropospheric wind and moisture distribution in Fig. 6 clarifies how the western North America region responds to the El Niño and the WWB. In Exp NW (Fig. 6a), the western

North America and the eastern Pacific regions are characterized by positive moisture anomalies with a strong on-shore moist flow. The inclusion of the WWB SST over the northeastern Pacific (Exp. CTL) shifts the distribution of cyclonic circulation anomalies over the northeastern Pacific northward (Fig. 6b). As shown in Fig. 7b, this northward shift is vertically linked to an enhancement of the negative SLP anomaly in response to the WWB SSTA located northward compared to the location of negative SLP anomaly along the western US coast in Fig. 7a, resulting in the enhanced cyclonic circulation anomalies close to Northwestern US and Southwestern Canada in Fig. 7d. Associated with these circulation anomalies, the simulation produces wet conditions (i.e., moist flow from the ocean and a positive humidity anomaly) over the Northwestern US and Southwestern Canada (Fig. 6b), which is consistent with the observed positive precipitation anomalies over that region during the 2015/16 winter (e.g., Fig. 2f). At the same time, the anticyclonic circulation anomalies to the south are associated with decreases in moisture over the southwest coast of the US and Mexico and a weak off-shore flow (Fig. 6b).

The SLP and upper-tropospheric (500mb) height and circulation fields also help to clarify how the atmosphere responds to the El Niño and WWB. The SLP field in Figure 7a shows a strong negative SLP anomaly over the northeastern Pacific with a positive anomaly to the southwest in the subtropical central Pacific. Another positive SLP anomaly is seen over the central Canada. Comparing the SLP anomalies to the upper-level height anomalies (Fig. 7c), one finds a slight westward tilt with height for the anomalies. Ascending motion is found on the southeastern side of the negative SLP anomaly over the Pacific (Fig. 7a), where the upper-level divergence between trough and ridge is expected. This region is connected with the low-level on-shore flow and humid conditions (Fig. 6a), associated with the above average precipitation over the Southwestern US (Fig. 5a).

The atmospheric structures shown in Figs. 7a,c produced in Exp NW are quite consistent with the typical tropospheric response to El Niño. When the effect of the WWB is added (Fig. 7b), there is an increase in SLP over the Southwestern US land, and a decrease in SLP and height over the northeastern Pacific. These changes in SLP and height and the corresponding changes in horizontal and vertical motion act to confine the west coast wet anomalies to Southwestern Canada and the Northwestern US (e.g., Figs. 5b and 6b).

Figures 5 through 7, along with quantitative estimation of the precipitation anomalies, overall demonstrate that the WWB acts to counter the El Niño-driven positive precipitation anomalies of 0.5–0.55 mm d^{-1} (Fig. 5a) over Southern California and Arizona, and part of Northwestern Mexico (110°–123°W, 25°–37°N), dropping that amount down to ~0.3 mm d^{-1} (Figs. 4b, 5b, 5c) though still insufficient to fully account for the observed negative precipitation anomalies of ~0.4 mm d^{-1} below average over that region (Fig. 2f). A significance test confirms that these two ensemble mean precipitation anomalies (from Exp. NW and Exp. CTL) are statistically different at 95 percent confidence level (indicated by dots in Fig. 5b). In the next section we examine the possible role of unforced atmospheric variability in further contributing to the observed below-average precipitation over that region[3].

5. The role of unforced atmospheric teleconnections

In section 4, we found that precipitation anomalies forced by the WWB are not sufficient to fully counteract the El Nino-driven positive precipitation anomalies simulated by the GEOS-5 AGCM in the Southwestern US (the difference between the ensemble mean of Exp CTL and the observations is shown in Fig. 8b). We also found that the upper-level negative geopotential

[3] Of course, we cannot rule out the possibility that the discrepancies between the observed and ensemble mean anomalies in part reflect model deficiencies in the AGCM response to SST.

height anomalies over the northeastern Pacific (while shifted north of those associated with the canonical El Niño response) are nevertheless still southeast of the observed (Fig. 8a). Over the Atlantic sector, the ensemble mean minus the observed z250 height anomaly shows negative anomalies over the Southeastern US and positive anomalies over the Northeastern Canada and Greenland suggesting a possible role of the NAO and/or AO (Fig. 8a).

In order to determine if the differences between observations and the ensemble mean response reflect contributions from internal modes of variability (i.e., modes unforced by SST), we investigate the intra-ensemble variability of the control (Exp CTL) simulations (following Hoerling and Kumar 1997). As shown in Fig. 9a, the intra-ensemble variance of geopotential height has local maxima over the northeastern Pacific, mid-latitude Atlantic, and Greenland areas. Relatively large variance is also seen over the Arctic. Interestingly, the areas of large intra-ensemble variance are indeed regions in which the NAO and AO teleconnection patterns are active. Large intra-ensemble variance of extra-tropical precipitation is primarily found over the western coastal region of North America and the mid-latitude Atlantic (Fig. 9b), consistent with the large variance of upper-level geopotential height over those regions. This suggests the possibility that unforced internal atmospheric noise components could contribute to the observed precipitation anomalies in those regions. We also show in Fig. 9 a rough measure of the signal to total variance (S/T) ratio computed as the square of the ensemble mean anomaly (the part forced by SST) divided by the sum of the square of the ensemble mean anomaly and intra-ensemble variance for both the 250mb geopotential height anomalies (Fig. 9c) and precipitation anomalies (Fig. 9d). This is our estimate of the fraction of the total variance forced by SST in the model results. The S/T values range from 0 to 1. Values greater than (equal to) 0.5 indicate that the magnitude of the part forced by SST is larger than (equal to) the unpredictable noise. The distribution of the height S/T values highlights the not unexpected large signal relative to the noise in the tropics. In the extratropics, the largest S/T values for the height field occur off-shore in the northeastern Pacific and over Canada, with the latter presumably being important for providing a predictable signal for the steering of storms into the west coast. The S/T ratio for the tropical precipitation shows the largest values just north of the equator near 140°W. In the middle latitudes a relative maximum occurs just off the west coast, while much of California has values ranging between 0.5 and 0.6. We note that the Eastern US has lower S/T values for precipitation than the Southwestern US (Fig. 9d), suggesting comparatively less predictability in that region.

To demonstrate that unforced internal atmospheric noise does indeed contribute to the observed precipitation anomalies, we next reconstruct the MERRA-2 geopotential height anomalies as a linear combination of the ensemble mean and the leading modes of the unforced atmospheric variability. A rotated empirical orthogonal function (REOF) (Richman 1986) is employed to capture the leading components of the unforced atmospheric variability from all 50 members of Exp CTL. As seen in the bottom panels of Fig. 10, the two leading modes do represent AO-like and NAO-like anomaly patterns (Figs. 10d,e). The third mode explains large variability across the mid- to high latitudes, showing some similarity to the NAO. We note that none of the first few leading modes resemble the PNA – suggesting that an influence that could be attributed to a different flavor of ENSO is weak in 2015. We will come back to the issue of the possible impact of a change in the character of ENSO in Section 6 (Fig. 13). The three leading modes account for ~65% of the intra-ensemble variance (30% (1st), 23% (2nd), and 14% (3rd)). We next use the leading REOFs as the predictors of the difference between observed anomaly and model's ensemble mean anomaly in a regression equation using the approach of

Chang et al. (2012). Figure 10c shows the reconstructed geopotential height anomalies as a sum of the ensemble mean and a linear combination of the first 3 independent leading modes of the unforced atmospheric variability. Comparing Figs. 10a-c, we see that the unforced components of atmospheric variability resembling the AO and NAO, which are not directly forced by SST (e.g., El Niño and the WWB), can account for a substantial portion of the observed height anomaly that is not reproduced by model's ensemble mean. The fact that very few of the leading modes of the intra-ensemble variance (together with the ensemble mean response) reconstruct the observed anomalies reasonably well suggests this is more than just a matter of the REOFs spanning the space of the observed variability, but that these REOFs represent physically realistic modes of variability present at that time (see also the last paragraph in this section regarding the associated precipitation anomalies including the month-to-month changes).

We next consider the intra-ensemble variability of the precipitation. In this case, rather than computing separate REOFs for the precipitation (which tend to be rather noisy) we simply regress the precipitation on the above leading height REOFs. The bottom panels of Fig. 11 (Figs. 11d–f) show the precipitation anomalies associated with the leading REOFs of the upper-level geopotential height anomalies (shown in Fig. 10). We find that the positive phase of all three REOFs are associated with negative precipitation anomalies over California region (McAfee and Russell 2008; Myoung et al. 2015). In particular, the upper-level positive height anomaly associated with the leading AO-like REOF (Fig. 10d) is linked to anomalous anticyclonic circulation and below-average moisture at 850mb (Fig. 12a) and the positive SLP anomaly and a strong subsidence along the west coast of the US (Fig. 12b). This leads to below-average precipitation over the Southwestern US region. For example, the reconstructed precipitation across the Southern California, Arizona, and part of Northwestern Mexico (110°–123°W, 25°–

37°N) in Fig. 11c demonstrates that the gap (~0.7 mm d^{-1}) between the observed negative precipitation anomalies (Fig. 11a) (~0.4 mm d^{-1} below average) and ensemble mean anomalies (Fig. 11b) (~0.3 mm d^{-1} above average) is narrowed to within 0.2 mm d^{-1} (area averaged difference: ~0.15 mm d^{-1}) by the contribution of the unforced components of atmospheric variability.

The above model results indicating a key role of unforced internal atmospheric modes of variability resembling the AO and NAO is not inconsistent with their observed phases during the 2015/16 winter. In particular, the indices of the NAO and AO (as provided by the NOAA Climate Prediction Center[4]) were both strong positive (2.2 and 1.4, respectively) in December followed by a weak positive phase for the NAO and strong negative phase for the AO in January (0.1 and –1.4). Monthly precipitation (MERRA-2) over the Southwestern US and Northwestern Mexico (110°–123°W, 25°–37°N) was below average (–0.5 mm d^{-1}) in December and above average (0.3 mm d^{-1}) in January, consistent with the expected impacts of the NAO/AO depending on their phases. Precipitation in February again dropped significantly down to –1.0 mm d^{-1}. The NAO during that month was in a strong positive phase (1.6), along with near zero amplitude of the AO (0.0), indicating that precipitation specifically during February 2016 could have been more affected by a positive phase of the NAO.

6. Remaining Issues and Discussion

This study employed the MERRA-2 reanalysis and GEOS-5 AGCM simulations with

---

[4] http://www.cpc.ncep.noaa.gov/products/precip/CWlink/daily_ao_index/monthly.ao.index.b50.current.ascii.table; http://www.cpc.ncep.noaa.gov/products/precip/CWlink/pna/norm.nao.monthly.b5001.current.ascii.table

specified SST to investigate the impact on the Western US 2015/16 winter climate of large-scale atmospheric teleconnections (both forced and unforced by SST). The AGCM experiments were designed to isolate the contribution from a persistent and strong WWB in the northeastern Pacific, and how that may have impacted the canonical response to a strong El Niño that was expected to bring (but failed to deliver) much-needed relief to the drought-stricken Southwest during that winter.

It was found that the atmospheric response to the WWB SST was indeed to decrease the precipitation in the Southwestern US region. This was accompanied by a reduction in moist transport, enhanced descending motion, and increased sea level pressure and anticyclonic circulation. In contrast, in the Northwestern US region the WWB produced anomalous cyclonic circulation and moist air transport from the Pacific, contributing to the enhancement of precipitation in that region.

It was further shown that, in the absence of the influence of the WWB, the response to the observed SST anomalies in all other regions was to produce wet conditions over the Southwest, similar to the canonical strong ENSO response. While the impact of the WWB (as described above) was to counteract the influence of El Niño in the Southwest, the model response to the WWB was not sufficient to fully overcome the relatively large El Nino-driven positive precipitation anomalies. There are a number of possible reasons for this including model errors, though we focused here on the role that unforced (by SST) atmospheric noise may have played in contributing to the precipitation deficit in the Southwest.

We estimated the contribution of the unforced atmospheric variability to the observed precipitation anomalies from the intra-ensemble variability of the model simulations. The analysis revealed that the leading modes of intra-ensemble variability of the 250mb height field have well-defined large-scale structures (with generally north/south oriented anomalies) that have some resemblance to the NAO and the AO patterns. It was further shown via a regression analysis that the three leading modes (together with the ensemble mean) could reproduce the observed height anomalies reasonably well, including the position of the negative anomaly in the northeast Pacific – a feature critical for obtaining the correct precipitation anomalies along the west coast. In fact, regressing the intra-ensemble variance of the precipitation against the leading height modes produced precipitation anomalies that did much to close the gap between the observed and ensemble mean response, especially in the Southwest where the AO-like and NAO-like leading noise pattern seem to play a key role.

To further bolster the above conclusions, a number of additional experiments were carried out to address issues concerning the sensitivity of the response to the character of the tropical Pacific SST, and the realism of the GEOS-5 AGCM response to El Niño.

The sensitivity of the response to the character of the tropical Pacific SST (i.e., the role of the different flavors of El Niño) was addressed with Exp SC (see Table 1 and description in Section 2.3). While the maximum SST anomalies in the equatorial Pacific did extend into the CP during 2015/16, a strong SST warming signal nevertheless also existed in the eastern Pacific. Fig. 13b shows that even when the 2015/16 tropical Pacific SST are confined to only those in the CP (with climatological SST everywhere else), positive precipitation anomalies were produced over California. This is in contrast to the response to the canonical CP El Niño (Fig. 13c), which produces much weaker (slightly positive) precipitation anomalies over California. We note that the eastern part of CP SST (180°–150°W) is larger in 2015/16 than in the historic CP El Niños, while the historic CP El Niño has larger warming than 2015/16 over the western part (160°E–180°) (Figure not shown). As such, the 2015/16 event was not a typical CP El Niño, though the maximum equatorial warming extended into the CP as noted above. Based on these results we conclude that the specific character (spatial distribution) of the tropical Pacific warming in 2015/16 is not a main cause of the negative precipitation anomalies in California.

In order to assess the realism of the AGCM's response to the strength of the tropical El Niño SST we carried out two additional sets of runs (Exp SS: see Table 1 and the description in Section 2.3), one in which the prescribed SST consisted of those from the 1997/98 El Niño (also a strong event but without a WWB), and another in which they consisted of an El Niño composite (the average of the years 1982, 86, 87, 91, 94, 97, 2002, 04, 06, and 09). The results (Fig. 14) show that during the strong 1997/98 El Niño the precipitation over the Southwestern US is substantially above average, consistent with the observations (cf. Figs. 14a,c). Negative precipitation anomalies are produced over part of the Northwestern US and Western Canada in both the simulation and observations (Figs. 14a,c). For the case of the El Niño composite SST, the model precipitation again shows positive anomalies over the Southwestern US with negative anomalies over the Northwestern US (Fig. 14b), though the magnitude of the wet anomaly over the Southwestern US is somewhat smaller than for the strong El Niño case (Figs. 14a,b). The distribution of the simulated precipitation anomalies is again quite realistic (cf. Figs. 14b,d). These results support our contention that the GEOS–5 AGCM responds reasonably well to El Niño SST strength, especially with respect to the wet conditions over the Southwestern US.

There is of course the more general question as to what extent model deficiencies may be impacting our conclusions. While we have shown that the combination of the response to the WWB and internal variability atmospheric variability acts to partly counter the precipitation response over the Southwestern US to the tropical El Niño SST, the observed precipitation anomaly, nevertheless, falls outside the 50 member ensemble spread (Fig. 5c), indicating model errors are also playing a role (Siler et al. 2017). This could for example be the result of bias in tropical convection (see Fig. 8b) that forces zonally-elongated mid-latitude height/circulation anomalies explaining some of height differences between observed and ensemble mean anomaly in mid-latitudes in Fig. 8a (e.g., Hoerling and Kumar 2003; Seager et al. 2003; Lau 2008). We also cannot rule out the possibility that the GEOS–5 model did not respond properly to non–ENSO tropical forcing such as that over the Warm Pool/Indian Ocean that has been shown to impact California precipitation (Seager et al. 2015).

The above discussion also gets to the question of predictability and prediction skill, and why almost all coupled models (including those from the National Multi-Model Ensemble (NMME) and the International Multi-Model Ensemble (IMME)) did not predict the continuation of the drought in Southern California (based on the ensemble averages), and in fact predicted the exact opposite (that there would be substantial relief from the drought in the form of positive precipitation anomalies presumably forced by the very strong El Nino-related tropical Pacific SST). To get further clarity on the NMME predictions, Fig. 15 shows Box and Whisker plots (analogous to Figs. 5c,d) for the SW and NW regions for seven of the NMME models. The results are for DJF 2015/16 for one-month lead-time, and based on 10 ensemble members for each model (https://iridl.ldeo.columbia.edu/SOURCES/.Models/.NMME). Focusing on the SW region, we see that all the models produce ensemble means that are positive (or near zero) with however several models having an ensemble spread large enough to encompass the observations. The differences among the models both in terms of the ensemble mean and spread suggest that model deficiencies are likely playing a role, though, consistent with our AGCM results, internal atmospheric variability could account for at least part of the observed anomaly. Regarding the role of the WWB, an inspection of the NMME SST predictions in the northeastern Pacific (http://www.cpc.ncep.noaa.gov/products/NMME/archive/2015110800/current/tmpsfc_Seas1.html) indicates these are reasonably well predicted at 1-month lead, suggesting that any such impact is likely well simulated by the NMME models (as found in our AGCM results (Exp CTL)), and therefore it is unlikely that deficiencies in the response to the WWB can account for the discrepancies in the precipitation responses.

Overall, the NMME results are not inconsistent with our results concerning the importance of internal atmospheric variability over the Southwestern US during the winter of 2015/16. As such, the fact that none of the NMME models predicted the negative precipitation anomalies (forecasting instead the strong and predictable response to the tropical Pacific SST forcing) is not too surprising, and may not represent a failure of the forecasts, but a failure to adequately provide the community with a quantifiable and understandable measure of the uncertainty in the predictions.

Acknowledgements

This work is supported by the NASA Modeling, Analysis, and Prediction (MAP) Program. The authors are grateful to anonymous reviewers for their helpful comments and suggestions.

References

Ashok, K., S. K. Behera, S. A. Rao, H. Weng, and T. Yamagata, 2007: El Niño Modoki and its possible teleconnections. *J. Geophys. Res.*, **112**, C11007, doi:10.1029/2006JC003798.

Bacmeister, J. T., M. J. Suarez, and F. R. Robertson, 2006: Rain reevaporation, boundary layerconvection interactions, and Pacific rainfall patterns in a AGCM. J.Atmos. Sci., 63, 33833403

Bacmeister, J. T., and G. Stephens, 2011: Spatial statistics of likely convective clouds in CloudSat data. *J. Geophys. Res*., **116**, D04104, doi:10.1029/2010JD014444.

Barahona, D., A. M. Molod, J. Bacmeister, A. Nenes, A. Gettelman, H. Morrison, V. Phillips, and A. Eichmann, 2014: Development of two-moment cloud microphysics for liquid and ice within the NASA Goddard Earth Observing System Model (GEOS-5). *Geosci. Model Dev*., **7**, 1733-1766, doi:10.5194/gmd-7-1733-2014.

Barnston, A. G., R. E. Livezey, and M. S. Halpert, 1991: Modulation of Southern Oscillation-Northern hemisphere mid-winter climate relationships by the QBO. *J. Climate,* **4**, 203-217.

Barsugli, J. J., and P. D. Sardeshmukh, 2002: Global atmospheric sensitivity to tropical SST anomalies throughout the Indo-Pacific basin. *J. Climate*, **15**, 3427-3442.

Bell, G. D., M. Halpert, and M. L´Heureux, 2016: ENSO and the tropical Pacific. *Bull. Amer. Meteor. Soc.*, **97**(8), S93-S98.

Blunden, J., and D. S. Arndt, Eds., 2016: State of the climate in 2015. *Bull. Amer. Meteor. Soc*., **97(8)**, S1-S275, doi:10.1175/2016BAMSStateoftheClimate.1

Bond, N. A., M. F. Cronin, H. Freeland, and N. Mantua, 2015: Causes and impacts of the 2014 warm anomaly in the NE Pacific. *Geophys. Res. Lett*., **42(9)**, doi:10.1002/2015GL063306.

Bosilovich, M. G., and coauthors, 2015: MERRA-2: Initial evaluation of the climate**.** *NASA/TM–2015–104606*, Vol. **43**, 139 pp.

Cai, W., and coauthors, 2014: Increasing frequency of extreme El Niño events due to greenhouse warming. *Nat. Climate Change*, **4**, 111-116, doi:10.1038/nclimate2100.

Capotondi, A., and coauthors, 2015: Understanding ENSO diversity. *Bull. Amer. Meteor. Soc*., **96**, 921-938, doi:10.1175/BAMS-D-13-00117.1.

Cayan, D. R., K. T. Redmond, and L. G. Riddle, 1999: ENSO and hydrologic extremes in the western United States. *J. Climate*, **12**, 2881-2893.

Chang, Y., S. D. Schubert, and M. Suarez, 2012: Attribution of the extreme U.S. East Coast snowstorm activity of 2010. *J. Climate*, **25**, 3771-3791. doi: 10.1175/JCLI-D-11-00353.1.

Donlon, C. J., M. Martin, J. D. Stark, J. Roberts-Jones, E. Fiedler and W. Wimmer, 2011: The

Operational Sea Surface Temperature and Sea Ice analysis (OSTIA). *Remote Sensing of the Environ.* doi: 10.1016/j.rse.2010.10.017 2011.

Garfinkel, C. I., and D. L. Hartmann, 2008: Different ENSO teleconnections and their effects on the stratospheric polar vortex. *J. Geophys. Res*., **113**, D18114, doi:10.1029/2008JD009920.

Ge, Y., G. Gong, and A. Frei, 2009: Physical mechanisms linking the winter Pacific-North American teleconnection pattern to spring North American snow depth. *J. Climate*, **21**, 5135-5148, doi:10.1175/2009JCLI2842.1.

Gelaro, R., and coauthors, 2017: The Modern-Era Retrospective Analysis for Research and Applications, Version-2 (MERRA-2). *J. Climate*, doi:10.1175/JCLI-D-16-0758.1, in press.

Global Modeling and Assimilation Office (GMAO), 2015a: MERRA-2 tavgM_2d_slv_Nx: 2d, Monthly mean, Time-Averaged, Single-Level, Assimilation, Assimilated Meteorological Fields, version 5.12.4, Greenbelt, MD, USA: Goddard Space Flight Center Distributed Active Archive Center (GSFC DAAC), Accessed Nov 2016. doi:10.5067/AP1B0BA5PD2K.

Global Modeling and Assimilation Office (GMAO), 2015b: MERRA-2 tavgM_2d_flx_Nx: 2d, Monthly mean, Time-Averaged, Single-Level, Assimilation, Surface Flux Diagnostics, version 5.12.4, Greenbelt, MD, USA: Goddard Space Flight Center Distributed Active Archive Center (GSFC DAAC), Accessed Nov 2016. doi:10.5067/0JRLVL8YV2Y4.

Global Modeling and Assimilation Office (GMAO), 2015c: MERRA-2 instM_3d_asm_Np: 3d, Monthly mean, Instantaneous, Pressure-Level, Assimilation, Assimilated Meteorological Fields, version 5.12.4, Greenbelt, MD, USA: Goddard Space Flight Center Distributed Active Archive Center (GSFC DAAC), Accessed Nov 2016. doi:10.5067/2E096JV59PK7.

Hoell, A., M. Hoerling, J. Eischeid, K. Wolter, R. Dole, J. Perlwitz, T. Xu, and L. Cheng, 2016: Does El Niño intensity matter for California precipitation? Geophys. Res. Lett., **43**, 819-825, doi:10.1002/2015GL067102.

Hoerling, M., and A. Kumar, 2003: The perfect ocean for drought. *Science*, **299**, 691-694, doi:10.1126/science.1079053.

Hoerling, M. P., and A. Kumar, 1997: Why do North American climate anomalies differ from one El Niño event to another? *Geophys. Res. Lett*., **24**, 1059-1062.

Hoerling, M. P., A. Kumar, and M. Zhong, 1997: El Niño, La Niña, and the nonlinearity of their teleconnections. *J. Climate*, 10, 1769-1786.

Hu, Z.-Z., A. Kumar, B. Jha, J. Zhu, and B. Huang, 2017: Persistence and predictions of the remarkable warm anomaly in the northeastern Pacific Ocean during 2014-16. *J. Climate*, **30**, 689-702, doi:10.1175/JCLI-D-16-0348.1.

Huang. B., M. L'Heureux, Z.-Z. Hu, and H.-M. Zhang, 2016: Ranking the strongest ENSO events while incorporating SST uncertainty. *Geophys. Res. Lett.*, **43**, 9165–9172, doi:10.1002/2016GL070888.

Jong, B.-T., M. Ting, and R. Seager, 2016: El Niño's impact on California precipitation: seasonality, regionality, and El Niño intensity. *Environ. Res. Lett.*, **11**, 054021, doi:10.1088/1748-9326/11/5/054021.

Kamae, Y., and coauthors, 2016: Forced response and internal variability of summer climate over western North America. *Clim. Dyn.*, online first, doi:10.1007/s00382-016-3350-x.

Kao, H.-Y., and J.-Y. Yu, 2009: Contrasting Eastern-Pacific and Central-Pacific types of ENSO. *J. Climate*, **22**, 615-632, doi:10.1175/2008JCLI2309.1.

Kim, S. T., and J.-Y. Yu, 2012: The two types of ENSO in CMIP5 models. *Geophys. Res. Lett.*, **39**, L11704, doi:10.1029/2012GL052006.

Koster, R. D., M. J. Suarez, A. Ducharne, M. Stieglitz, and P. Kumar, 2000: A catchment-based approach to modeling land surface processes in a general model: 1. Model structure. *J. Geophys. Res.*, **105(D20)**, 24809-24822, doi:10.1029/2000JD900327.

Kug, J.-S., F.-F. Jin, and S.-I. An, 2009: Two-types of El Niño events: Cold tongue El Niño and warm pool El Niño. *J. Climate*, **22**, 1499–1515, doi:10.1175/2008JCLI2624.1.

Larkin, N. K., and D. E. Harrison, 2005: Global seasonal temperature and precipitation anomalies during El Niño autumn and winter. *Geophys. Res. Lett.*, **32**, L16705, doi:10.1029/2005GL022860.

Lau, N.-C., A. Leetmaa, and M. J. Nath, 2008: Interactions between the responses of North American climate to El Niño-La Niña and to the secular warming trend in the Indian-western Pacific oceans. *J. Climate*, **21**, 476-494, doi:10.1175/2007JCLI1899.1.

Leathers, D. J., B. Yarnal, and M. A. Palecki, 1991: The Pacific/North American teleconnection pattern and United States climate. Part I: Regional temperature and precipitation associations. *J. Climate*, **4**, 517-528.

L'Heureux, M., K. Takahashi, A. Watkins, A. Barnston, E. Becker, T. Di Liberto, F. Gamble, J. Gottschalck, M. Halpert, B. Huang, K. Mosquera-Vásquez, and A. Wittenberg, 2016: Observing and Predicting the 2015-16 El Niño. *Bull. Amer. Meteor. Soc.*, doi: 10.1175/BAMS-D-16-0009.1., in press.

Lim, Y.-K., R. Kovach, S. Pawson, and G. Vernieres, 2017: The 2015/2016 El Niño event in context of the MERRA-2 reanalysis: A comparison of the tropical Pacific with 1982/1983 and 1997/1998. *J. Climate*, **30**, 4819-4842, doi:10.1175/JCLI-D-16-0800.1.

Lim, Y.-K., S. D. Schubert, O. Reales, M.-Y. Lee, A. M. Molod, and M. J. Suarez, 2015: Sensitivity of tropical cyclones to parameterized convection in the NASA GEOS5 model. *J. Climate*, **28**, 551-573, doi:10.1175/JCLI-D-14-00104.1.

Lorenzo, E. D., and N. Mantua, 2016: Multi-year persistence of the 2014/15 North Pacific marine heatwave. *Nature Climate Change*, **6**, 1042-1047, doi:10.1038/nclimate3082.

Mantua N. J., S. R. Hare, Y. Zhang, J. M. Wallace, and R. C. Francis, 1997: A Pacific interdecadal climate oscillation with impacts on salmon production. *Bull. Amer. Meteor. Soc*., **78**, 1069-1079.

McAfee, S. A., and J. L. Russell, 2008: Northern annular mode impact on spring climate in the western United States. *Geophys. Res. Lett*., **35**, L17701, doi:10.1029/2008GL034828.

Mo, K., and R. E. Livezey, 1986: Tropical-extratropical geopotential height teleconnections during the Northern hemisphere winter. *Mon. Wea. Rev*., **114**, 2488-2515.

Mo, K., 2010: Interdecadal modulation of the impact of ENSO on precipitation and temperature over the United States. *J. Clim*., **23**, 3639-3656.

Molod, A. M., L. Takacs, M. Suarez, and J. Bacmeister, 2015: Development of the GEOS-5 atmospheric general circulation model: evolution from MERRA to MERRA2. *Geosci. Model Dev.*, **8**, 1339-1356, doi:10.5194/gmd-8-1339-2015.

Moorthi, S., and M. J. Suarez, 1992: Relaxed Arakawa-Schubert: A parameterization of moist convection for general circulation models. *Mon. Wea. Rev*., **120**, 978-1002.

Myoung, B., S.-H. Kim, J. Kim, and M. C. Kafatos, 2015: On the relationship between the North Atlantic Oscillation and early warm season temperatures in the southwestern United States. *J. Climate*, **28**, 5683-5698, doi:10.1175/JCLI-D-14-00521.1.

Opar, A., 2015: Lost at sea: Starving birds in a warming world. *Audubon Magazine*, March-April, https://www.audubon.org/magazine/march-april-2015/lost-sea-starving-birds-warming-world

Reynolds, R. W., T. M. Smith, C. Liu, D. B. Chelton, K. S. Casey, and M. G. Schlax, 2007: Daily high-resolution-blended analyses for sea surface temperature. *J. Climate*, **20**, 5473-5496, doi:10.1175/2007JCLI1824.1.

Richman, M. B., 1986: Rotation of principal components. *J. Climatol*. **6**, 293–335.

Rienecker, M. M., and coauthors, 2008: The GEOS-5 data assimilation system-documentation of version 5.0.1 and 5.1.0, and 5.2.0. NASA Tech. Rep. Series on Global Modeling and Data

Assimilation, NASA/TM-2008-104606, **27**, 92pp.

Rienecker, M.M., and Coauthors, 2011: MERRA - NASA's Modern-Era Retrospective Analysis for Research and Applications. *J. Climate*, **24**, 3624-3648. doi: 10.1175/JCLI-D-11-00015.1.

Ropelewski, C. F., and M. S. Halpert, 1986: North American precipitation and temperature patterns associated with the El Niño/Southern Oscillation (ENSO). Mon. Wea. Rev., 114, 2352-2362.

Schubert, S. D., and Y.-K. Lim, 2013: Climate variability and weather extremes: model simulated and historical data. Chapter 9 in a book entitled “Extremes in a changing climate: Detection, analysis, and uncertainty” by Sorooshian et. al. editors., Water Science and Technology Library 65, doi:10.1007/978-94-007-4479-0_9, Springer, 239-285.

Seager, R., N. Harnik, Y. Kushnir, W. Robinson, and J. Miller, 2003: Mechanisms of hemispherically symmetric climate variability. *J. Climate*, **16**, 2960-2978.

Seager, R., Y. Kushnir, C. Herweijer, N. Naik, and J. Velez, 2005: Modeling of tropical forcing of persistent droughts and pluvials over western North America: 1856–2000. J. Climate, **18**, 4065–4088, doi:10.1175/JCLI3522.1.

Seager, R., M. Hoerling, S. Schubert, H. Wang, B. Lyon, A. Kumar, J. Nakamura, and N. Henderson, 2015: Causes of the 2011–14 California Drought. *J. Climate*, **28**, 6997–7024, doi: 10.1175/JCLI-D-14-00860.1.

Siler, N., Y. Kosaka, S.-P. Xie, and X. Li, 2017: Tropical ocean contributions to California’s surprisingly dry El Niño of 2015/16. *J. Climate*, **30**, 10067-10079, doi:10.1175/JCLI-D-17-0177.1.

Simmons, A., J. M. Wallace, and G. Branstator, 1983: Barotropic wave propagation and instability, and atmospheric teleconnection patterns. *J. Atmos. Sci*., **40**, 1363–1392.

Straus, D. M., and J. Shukla, 2002: Does ENSO force the PNA? *J. Climate*, **15**, 2340–2358.

Thompson, D. W. J., and J. M. Wallace, 1998: The Arctic Oscillation signature in the wintertime geopotential height and temperature fields. *Geophys. Res. Lett*., **25**, 1297-1300.

Tokioka, T., K. Yamazaki, A. Kitoh, and T. Ose, 1988: The equatorial 30–60 day oscillation and the Arakawa-Schubert penetrative cumulus parameterization, *J. Meteorol. Soc. Japan*., **66**, 883–901.

Trenberth, K. E., G. W. Branstator, D. Karoly, A. Kumar, N-C. Lau, and C. Ropelewski, 1998: Progress during TOGA in understanding and modeling global teleconnections associated with tropical sea surface temperatures. *J. Geophys. Res.*, **103**, 14291-14324.

Woodhouse, C. A., 2003: A 431-yr reconstruction of western Colorado snowpack from tree rings. *J. Climate*, **16**, 1551-1561.

Whitney, F. A., 2015: Anomalous winter winds decreases 2014 transition zone productivity in the NE Pacific. *Geophys. Res. Lett*., **42**, 428–431, doi:10.1002/2014GL062634.

Yeh, S.-W., J.-S. Kug, B. Dewitte, M.-H. Kwon, B. Kirtman, and F.-F. Jin, 2009: El Niño in a changing climate. *Nature*, **461**, doi:10.1038/nature08316.

Yu, B., 2007: The Pacific–North American pattern associated diabatic heating and its relationship to ENSO. *Atmos. Sci. Lett.*, **8**, 107-112.

Yu, J.-Y., Y. Zou, S.-T. Kim, and T. Lee, 2012: The changing impact of El Niño on US winter temperatures. *Geophys. Res. Lett*., **39**, L15702, doi:10.1029/2012GL052483.

Yu, J.-Y. and Y. Zou, 2013: The enhanced drying effect of Central-Pacific El Nino on US winter. *Environ. Res. Lett*., **8**, 014019, doi:10.1088/1748-9326/8/1/014019.

Table 1. Summary of the main and the auxiliary experiments carried out in this study.

	Exp. Name	Prescribed SST	Information	members
Main Exp.	CTL	Obs. 2015/16 SST everywhere	El Niño & WWB effect	50
	NW	Same SST as Exp CTL but for the 2015/16 El Niño associated SST over the northeastern Pacific	El Niño, but no WWB effect	50
	CLIM	SST are climatological (1980-2015) everywhere	no El Niño no WWB effect	20
Auxiliary Exp.	SC	A: Obs. 2015/16 SST over the entire equatorial Pacific	2015/16 El Niño effect from both EP and CP warming	10
		B: Obs. 2015/16 SST over the central equatorial Pacific (160°E–150°W, Niño 4 region) only	CP warming effect in 2015/16 El Niño	10
		C: SST composite of the recent CP El Niño events over the central equatorial Pacific only	CP warming effect in the CP El Niños	10
	SS	A: Obs. 1997/98 SST everywhere	1997/98 El Niño	10
		B: Historic mean El Niño SST everywhere	El Niño effect from historic mean El Niño SST	10

Figure Captions

Figure 1. Pacific domain that depicts how the SST is prescribed for Exp NW (left) and Exp CTL (right), respectively. Exp CTL has the observed SST prescribed globally, while Exp NW differs only from Exp CTL in that the SST in the region of the WWB are set to only the 2015/16 El Niño-associated SST to remove the warmer SST associated with the northeastern Pacific WWB. Shaded is the smoothed SST anomaly distribution averaged over the simulation period from July 2015 through February 2016. See text for details.

Figure 2. Distributions of the MERRA-2 2-meter air temperature anomalies [K] (left) and precipitation anomalies [mm d^{-1}] (right) for three strongest El Niño winters (DJF). They are, from the top to the bottom, 1982/1983, 1997/1998, and 2015/2016.

Figure 3. Upper: Anomalous distribution of the SLP [mb] (left), 850mb specific humidity [10^{-1} g/kg] and horizontal wind [m s^{-1}] (middle), and 250mb geopotential height [m] (right) from the MERRA-2 for DJF 2015/2016. Lower: The observed sea surface temperature anomalies [K] in JJA 2015 (left) and DJF 2015/2016 (right).

Figure 4. 250mb geopotential height anomalies [m] (left, shaded) and precipitation anomalies [mm d^{-1}] (right) for DJF 2015/2016 produced by the GEOS-5 AGCM forced with observed SST prescribed globally (Exp CTL – Exp CLIM). Contour lines on the left panel denote the 250mb geopotential height [m] anomalies from MERRA-2.

Figure 5. Precipitation [mm d^{-1}] fields for DJF 2015/2016 reproduced by the experiments. Panel a) represents the precipitation from the Exp NW minus Exp CLIM. Panel b) represents the Exp CTL minus Exp NW, explaining the precipitation change by the addition of the WWB effect to the El Niño effect. Dots are plotted at the grid points, where the difference between the two ensemble means is significant at the 95 percent confidence level, based on a t-test. Bottom panel: Box-whisker plots of the DJF 2015/16 precipitation anomalies from Exp CTL (red) and Exp NW (blue) for the Southern California, Arizona, and Northwestern Mexico (110°–123°W, 25°–37°N) (left panel) and the Northwestern US and Southwestern Canada (120°–130°W, 38°–55°N) (right panel). Horizontal lines in the boxes denote the 1st quartile (bottom edge), median (inside boxes), and 3rd quartile (top edge). Crosses inside boxes are the mean, and the whiskers represent spread of model ensemble. Horizontal orange lines are the observed precipitation anomalies.

Figure 6. Same as upper panel in Fig. 5 but for the 850-950mb averaged specific humidity [10^{-1}

g/kg] and 850mb horizontal wind [m s^{-1}].

Figure 7. Same as upper panel in Fig. 5 but for SLP [mb] (shaded) and 500mb omega velocity [10^{-2} Pa s^{-1}] (contoured) (upper panels) and 500mb geopotential height and horizontal circulation (lower panels).

Figure 8. Difference in geopotential height (left) and precipitation (right) between model's ensemble mean from Exp CTL and observation (model minus observation) for DJF 2015/2016.

Figure 9. The intraensemble standard deviation of a) the 250mb geopotential height anomalies [m] and b) precipitation [mm d^{-1}] from Exp CTL.   The ratio of the square of the ensemble mean anomaly to the total variance (the square of the ensemble mean anomaly (Exp CTL – Exp CLIM) plus the intra-ensemble variance) of c) the 250mb geopotential height anomalies and d) precipitation. Units: dimensionless.

Figure 10. Distribution of the 250mb geopotential height anomalies [m] from MERRA-2 (a), model's ensemble mean (b), reconstruction as a linear combination of model's ensemble mean and unforced components of atmospheric variability (c), and the leading REOFs (positive phase basis) of those unforced components (d)–(f).

Figure 11. Same as Fig. 10 but for precipitation [mm d^{-1}].

Figure 12. Regressed REOFs onto the AO-like REOF of the 250mb geopotential height anomalies (Fig. 10d). The key atmospheric variables used for this regression are 850mb specific humidity [10^{-1} g/kg] and circulation [m s^{-1}] (left), and SLP [mb] and 500mb omega velocity [10^{-2} Pa s^{-1}] (right).

Figure 13. Precipitation anomalies [mm d^{-1}] for DJF period produced by the experiments (Exp SC, see Section 2.3 and Table 1). Exp SC-A is the experiment with observed 2015/16 SST prescribed over the tropical Pacific (10°S – 20°N) only. Exp SC-B is the same as Exp SC-A but for prescribing observed 2015/16 SST over the central tropical Pacific (160°E–150°W, Niño 4 region) only. Exp SC-C is the same as Exp SC-B but for observed SST composite over the central tropical Pacific from historic CP El Niño events that occurred in 1987, 91, 94, 2002, 04, and 09. SSTs in everywhere else are climatology. Each panel depicts precipitation anomalies of "Exp SC-A minus Exp CLIM" (left), "Exp SC-B minus Exp CLIM" (middle), and "Exp SC-C minus Exp CLIM" (right).

Figure 14. Comparison in DJF precipitation anomalies [mm d^{-1}] between model simulations (upper) (Exp SS, see Section 2.3 and Table 1) and MERRA-2 (lower). The upper-left panel

corresponds to the precipitation for a strong 1997/98 El Niño (Exp SS-A), while the upper-right panel is for all historic El Niño composite (1982, 86, 87, 91, 94, 97, 2002, 04, 06, and 09) (Exp SS-B).

Figure 15. Box-whisker plots of the predicted DJF 2015/16 precipitation anomalies (initialized in November) from the NMME participating models. The left panel is for the precipitation anomaly for the Southern California, Arizona, and Northwestern Mexico (110°–123°W, 25°–37°N) region, while the precipitation on the right panel represents the Northwestern US and Southwestern Canada (120°–130°W, 38°–55°N) region. Horizontal lines in the boxes denote the 1st quartile (bottom edge), median (inside boxes), and 3rd quartile (top edge). Crosses inside boxes are the mean, and the whiskers represent spread of model ensemble. Horizontal orange lines are the observed precipitation anomalies.

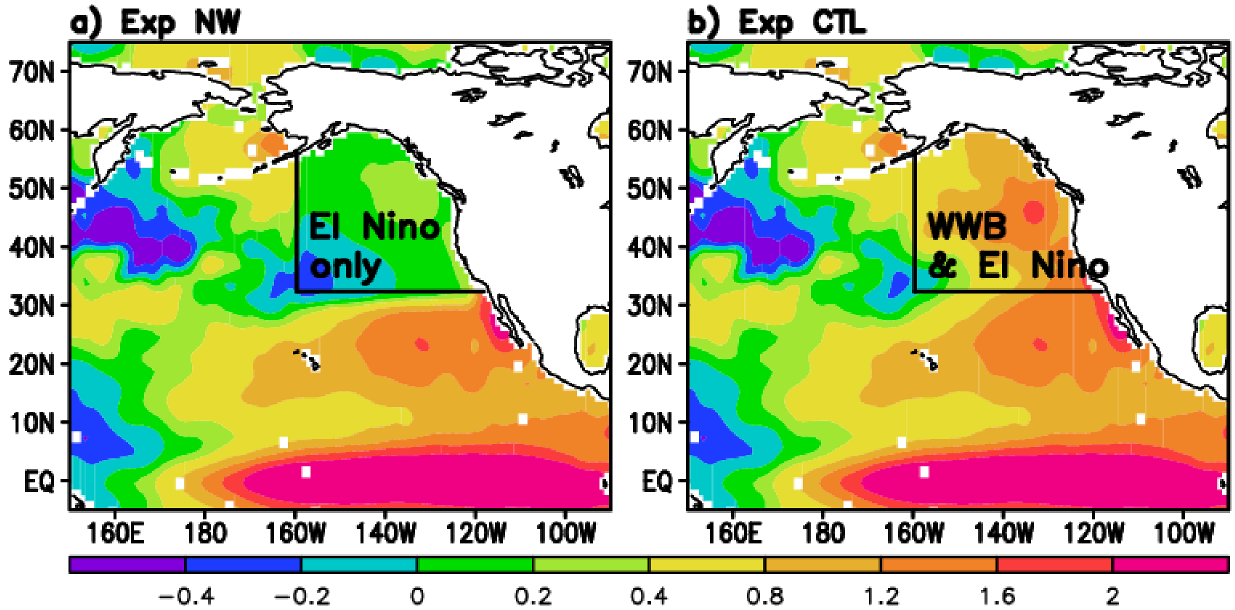

Figure 1. Pacific domain that depicts how the SST is prescribed for Exp NW (left) and Exp CTL (right), respectively. Exp CTL has the observed SST prescribed globally, while Exp NW differs only from Exp CTL in that the SST in the region of the WWB are set to only the 2015/16 El Niño-associated SST to remove the warmer SST associated with the northeastern Pacific WWB. Shaded is the smoothed SST anomaly distribution averaged over the simulation period from July 2015 through February 2016. See text for details

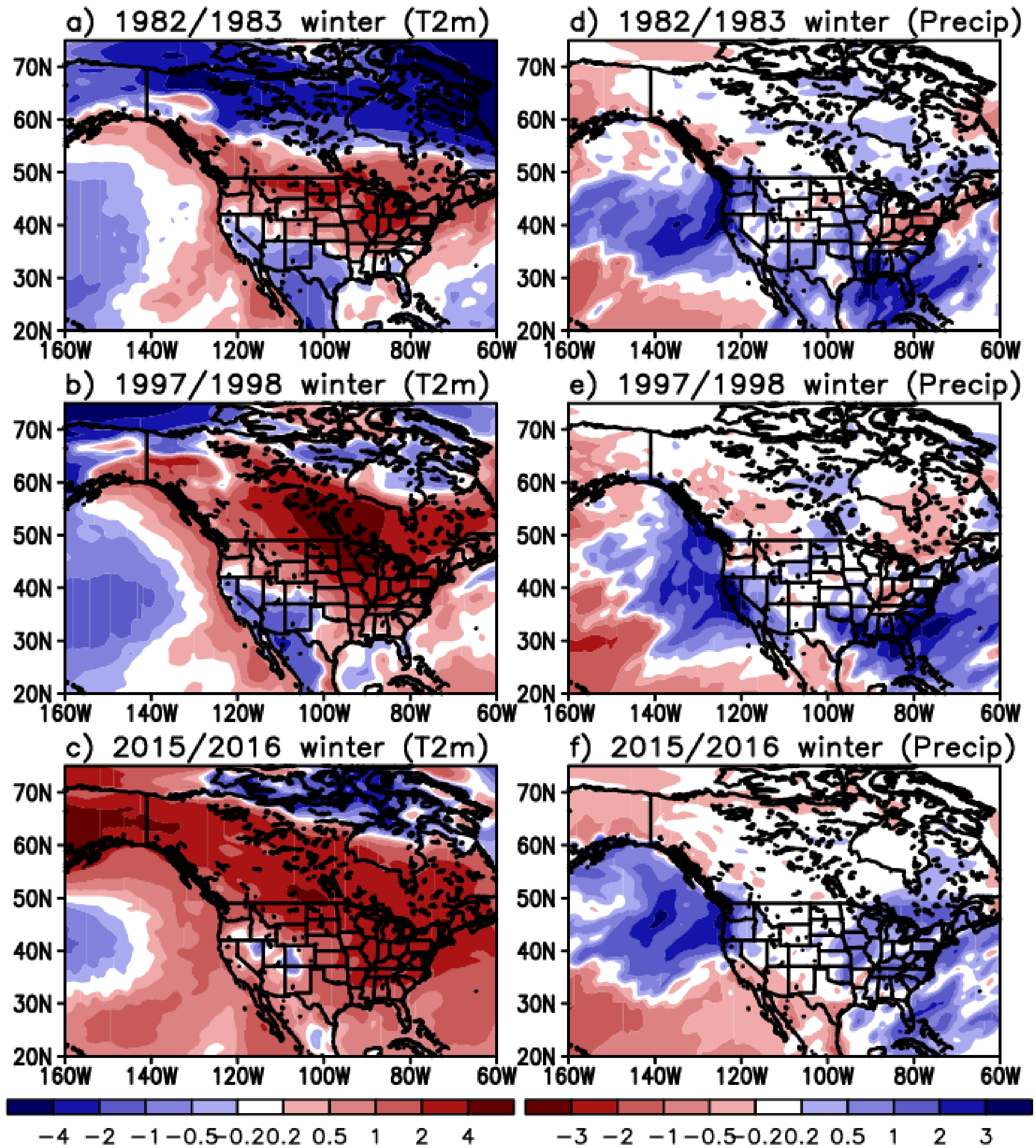

Figure 2. Distributions of the MERRA-2 2-meter air temperature anomalies [K] (left) and precipitation anomalies [mm d^{-1}] (right) for three strongest El Niño winters (DJF). They are, from the top to the bottom, 1982/1983, 1997/1998, and 2015/2016.

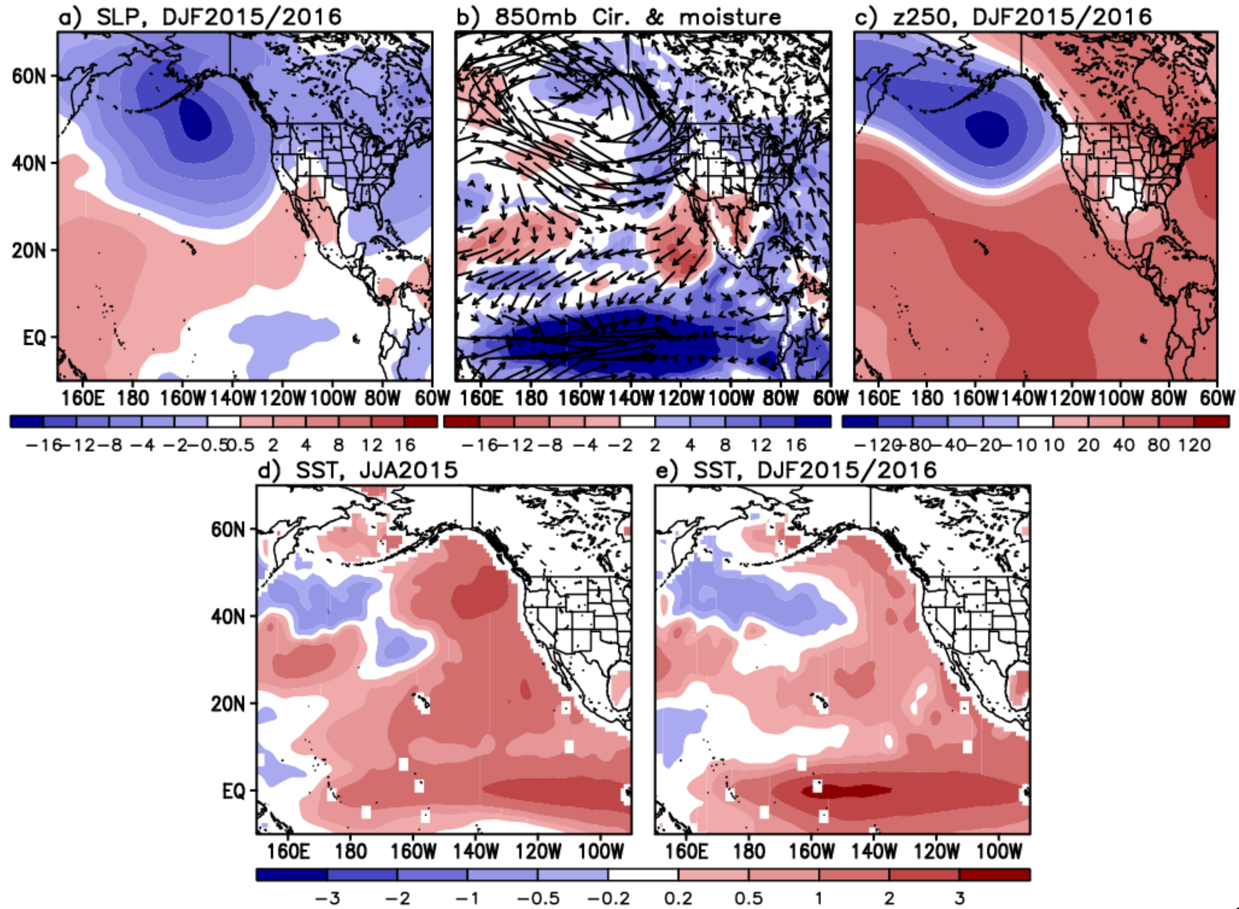

Figure 3. Upper: Anomalous distribution of the SLP [mb] (left), 850mb specific humidity [10^{-1} g/kg] and horizontal wind [m s^{-1}] (middle), and 250mb geopotential height [m] (right) from the MERRA-2 for DJF 2015/2016. Lower: The observed sea surface temperature anomalies [K] in JJA 2015 (left) and DJF 2015/2016 (right).

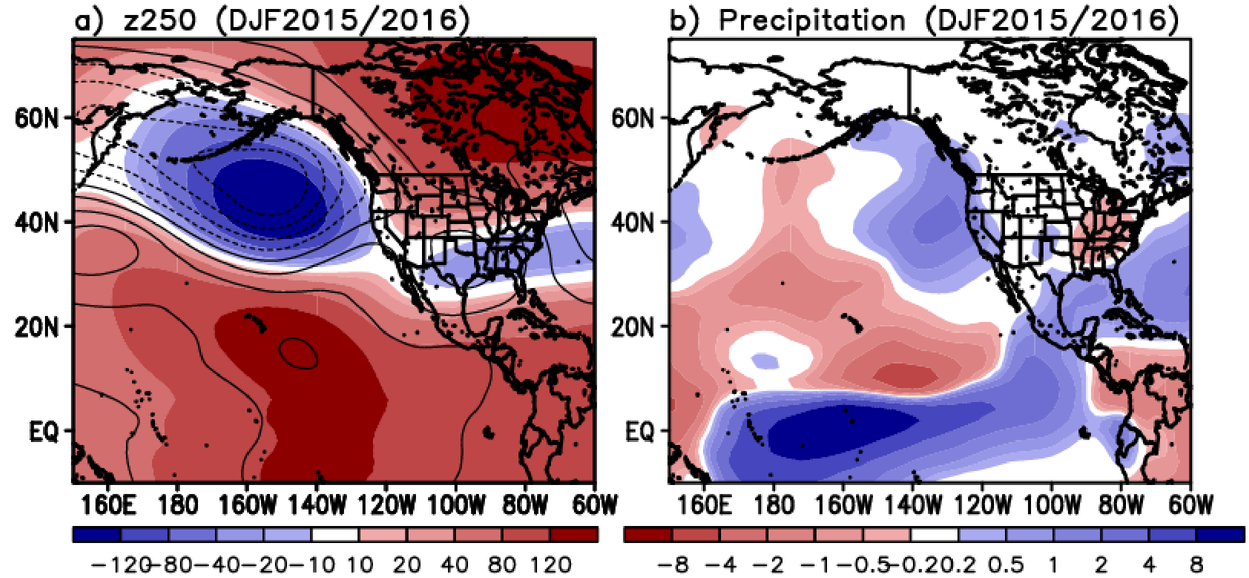

Figure 4. 250mb geopotential height anomalies [m] (left, shaded) and precipitation anomalies [mm d^{-1}] (right) for DJF 2015/2016 produced by the GEOS-5 AGCM forced with observed SST prescribed globally (Exp CTL – Exp CLIM). Contour lines on the left panel denote the 250mb geopotential height [m] anomalies from MERRA-2.

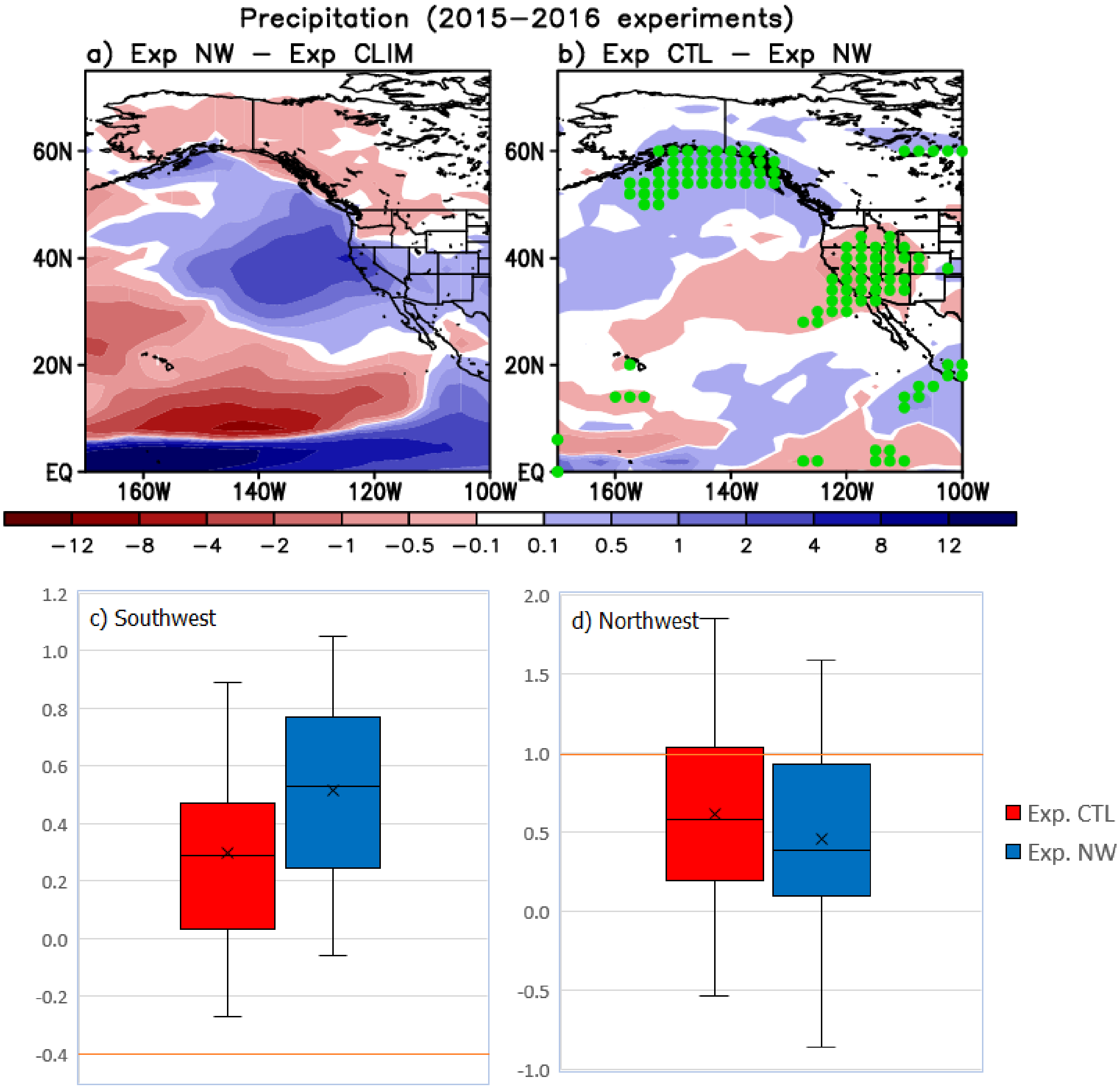

Figure 5. Precipitation [mm d^{-1}] fields for DJF 2015/2016 reproduced by the experiments. Panel a) represents the precipitation from the Exp NW minus Exp CLIM. Panel b) represents the Exp CTL minus Exp NW, explaining the precipitation change by the addition of the WWB effect to the El Niño effect. Dots are plotted at the grid points, where the difference between the two ensemble means is significant at the 95 percent confidence level, based on a t-test. Bottom panel: Box-whisker plots of the DJF 2015/16 precipitation anomalies from Exp CTL (red) and Exp NW (blue) for the Southern California, Arizona, and Northwestern Mexico (110°–123°W, 25°–37°N) (left panel) and the Northwestern US and Southwestern Canada (120°–130°W, 38°–55°N) (right panel). Horizontal lines in the boxes denote the 1st quartile (bottom edge), median (inside boxes), and 3rd quartile (top edge). Crosses inside boxes are the mean, and the whiskers represent spread of model ensemble. Horizontal orange lines are the observed precipitation anomalies.

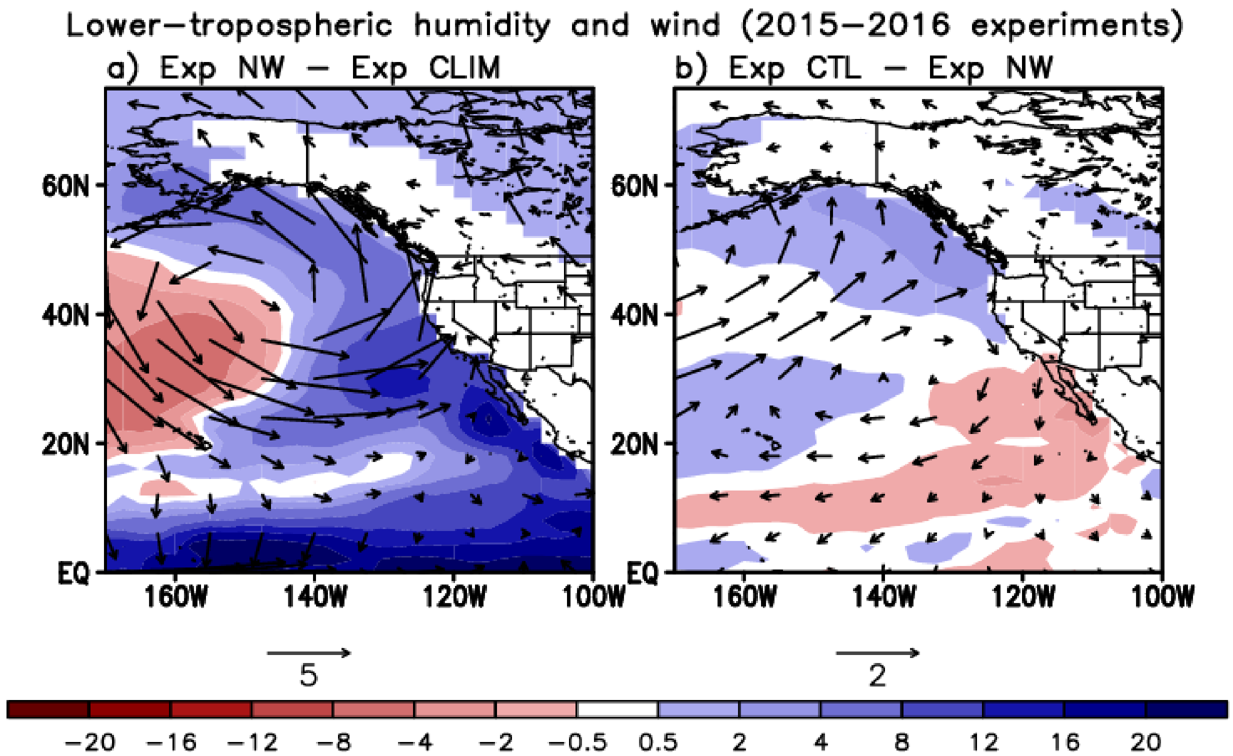

Figure 6. Same as upper panel in Fig. 5 but for the 850-950mb averaged specific humidity [10^{-1} g/kg] and 850mb horizontal wind [m s^{-1}].

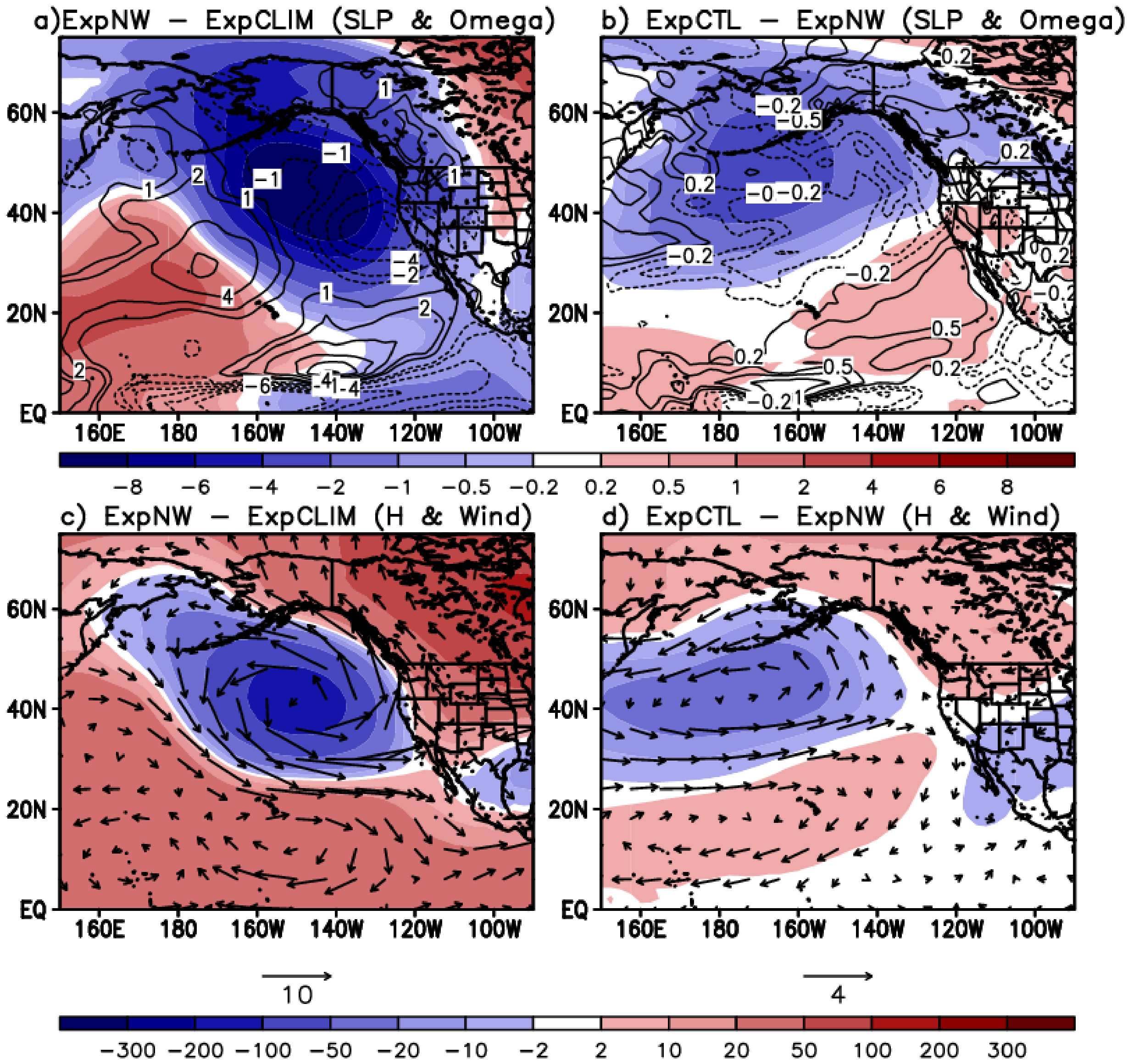

Figure 7. Same as upper panel in Fig. 5 but for SLP [mb] (shaded) and 500mb omega velocity [10^{-2} Pa s^{-1}] (contoured) (upper panels) and 500mb geopotential height and horizontal circulation (lower panels).

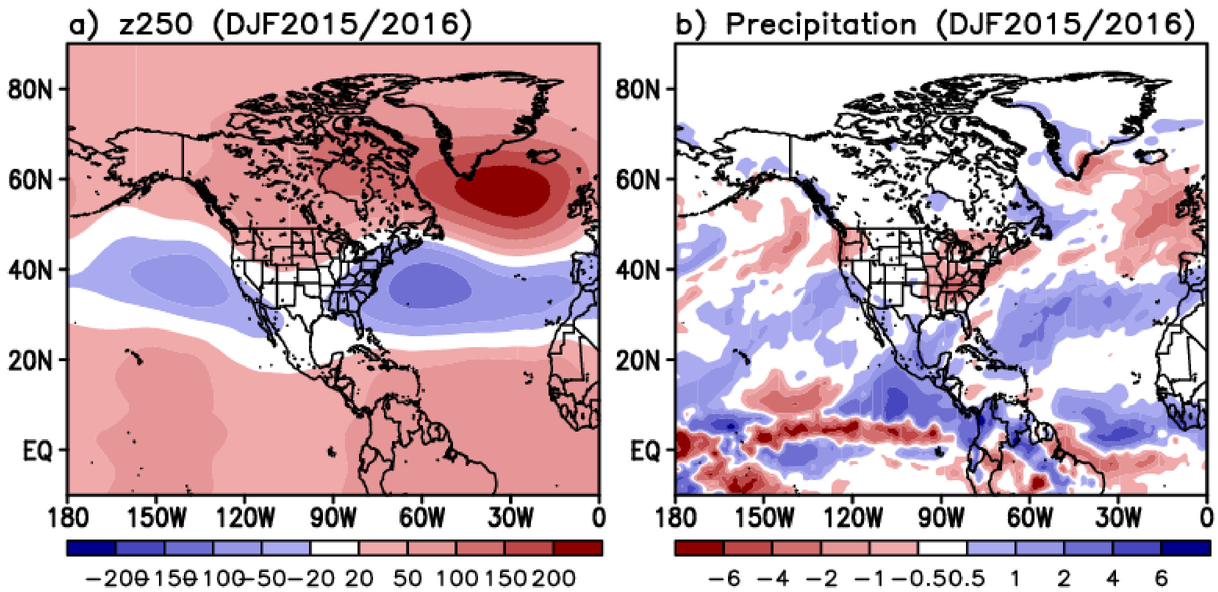

Figure 8. Difference in geopotential height (left) and precipitation (right) between model's ensemble mean from Exp CTL and observation (model minus observation) for DJF 2015/2016.

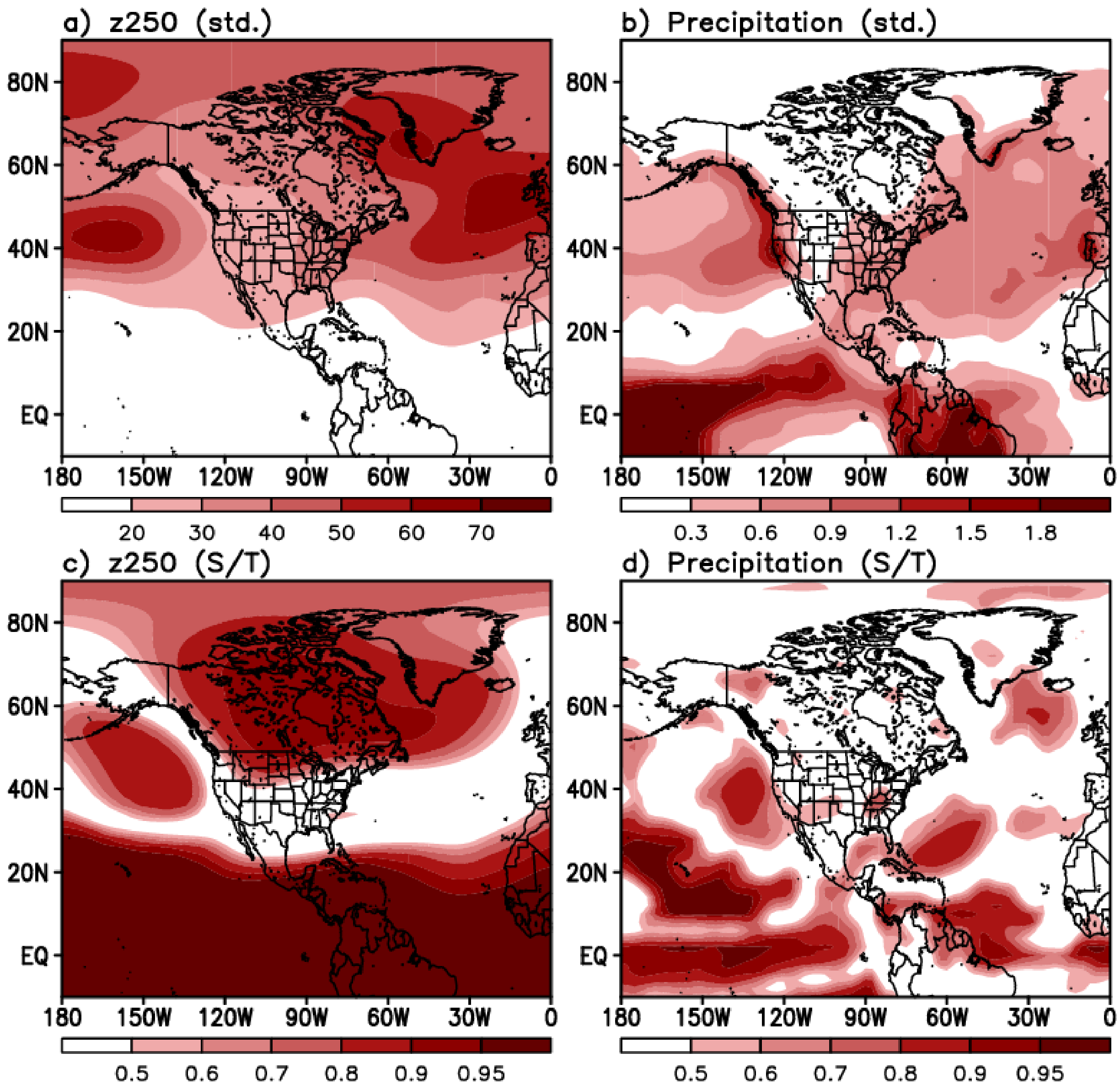

Figure 9. The intraensemble standard deviation of a) the 250mb geopotential height anomalies [m] and b) precipitation [mm d^{-1}] from Exp CTL. The ratio of the square of the ensemble mean anomaly to the total variance (the square of the ensemble mean anomaly (Exp CTL – Exp CLIM) plus the intra-ensemble variance) of c) the 250mb geopotential height anomalies and d) precipitation. Units: dimensionless.

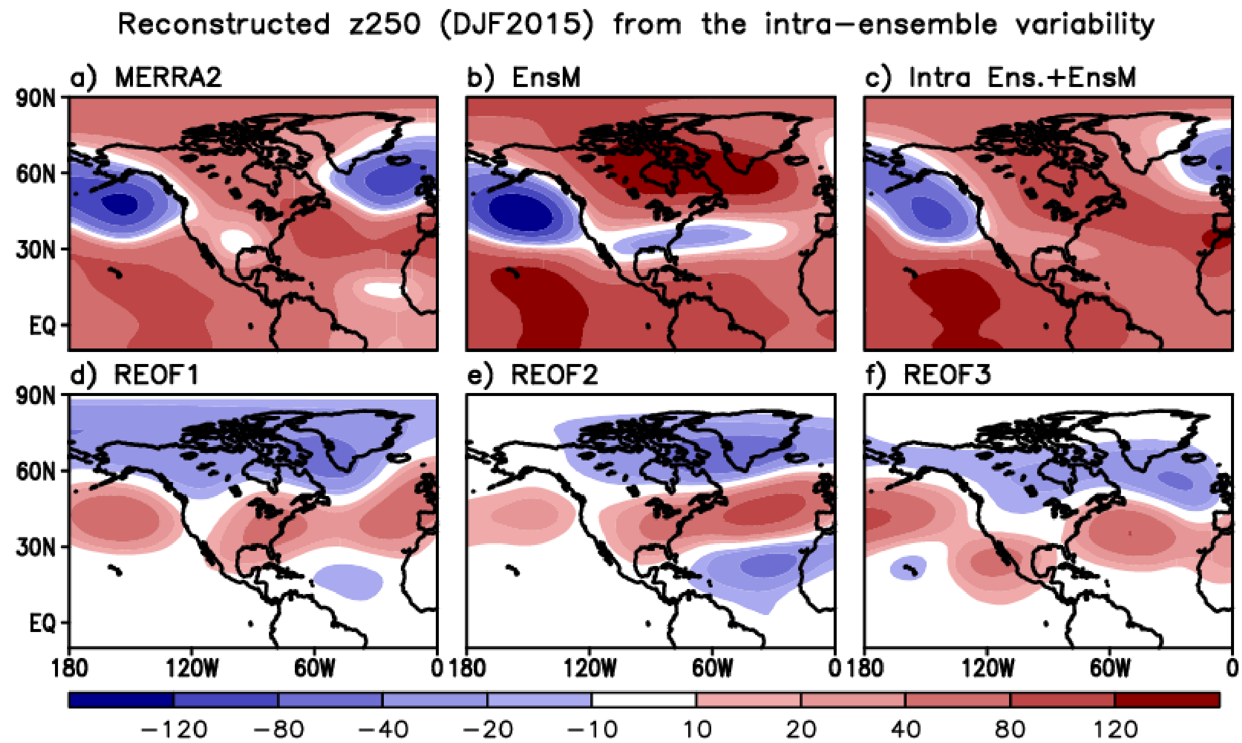

Figure 10. Distribution of the 250mb geopotential height anomalies [m] from MERRA-2 (a), model's ensemble mean (b), reconstruction as a linear combination of model's ensemble mean and unforced components of atmospheric variability (c), and the leading REOFs (positive phase basis) of those unforced components (d)–(f).

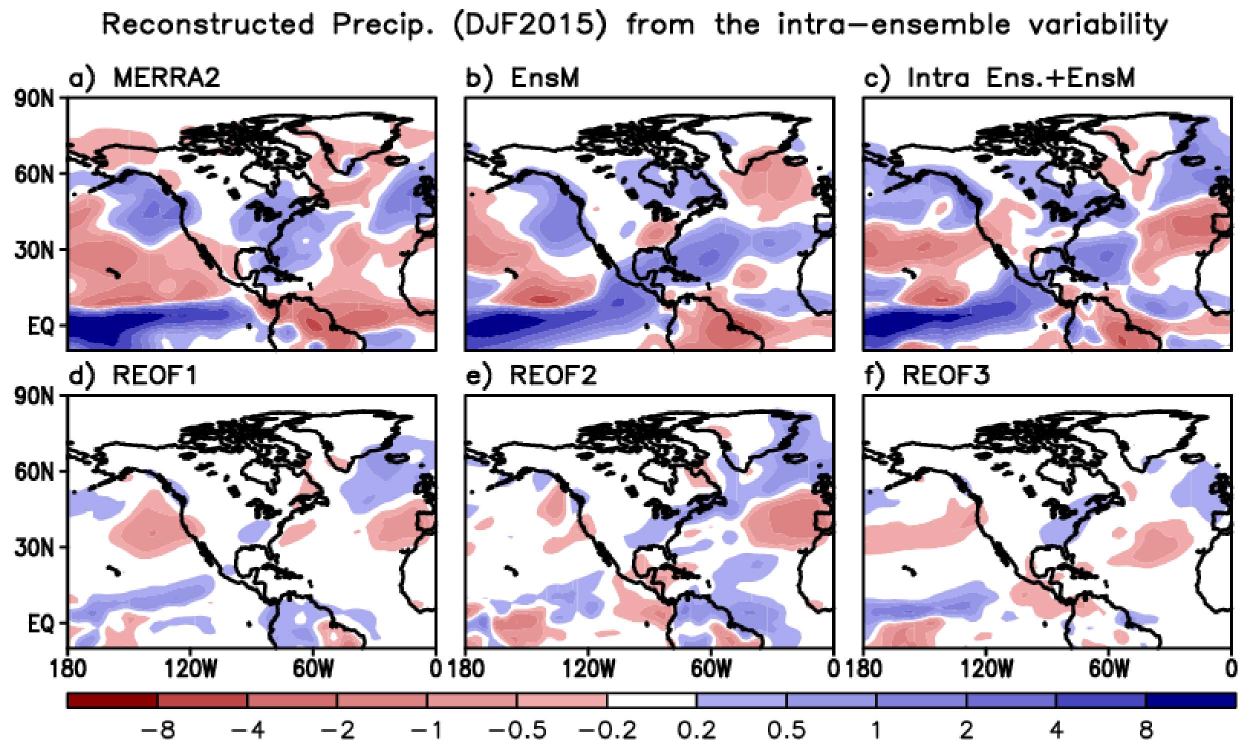

Figure 11. Same as Fig. 10 but for precipitation [mm d^{-1}].

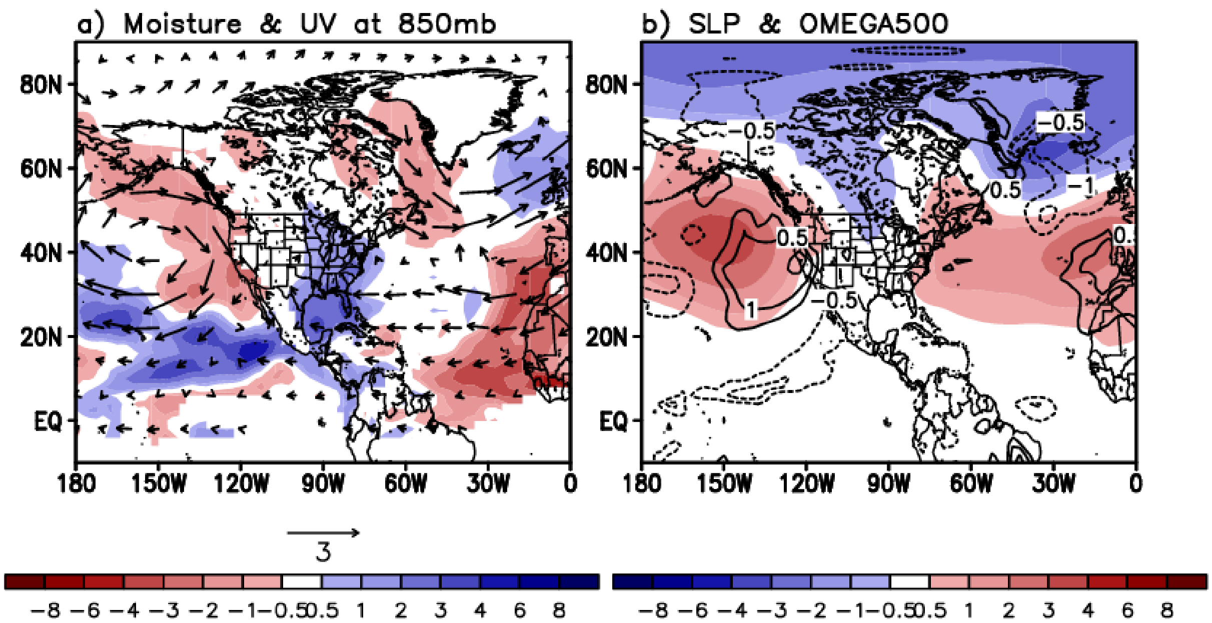

Figure 12. Regressed REOFs onto the AO-like REOF of the 250mb geopotential height anomalies (Fig. 10d). The key atmospheric variables used for this regression are 850mb specific humidity [10^{-1} g/kg] and circulation [m s^{-1}] (left), and SLP [mb] and 500mb omega velocity [10^{-2} Pa s^{-1}] (right).

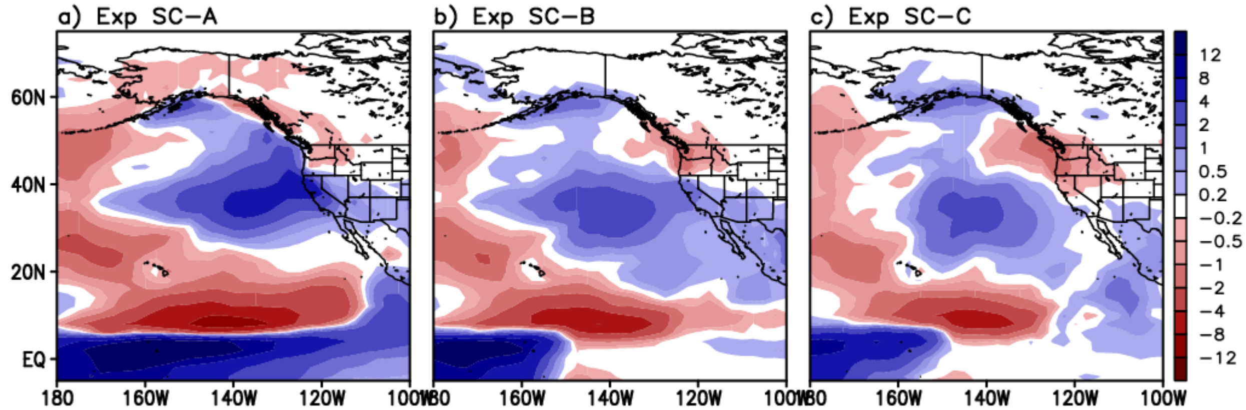

Figure 13. Precipitation anomalies [mm d^{-1}] for DJF period produced by the experiments (Exp SC, see Section 2.3 and Table 1). Exp SC-A is the experiment with observed 2015/16 SST prescribed over the tropical Pacific (10°S – 20°N) only. Exp SC-B is the same as Exp SC-A but for prescribing observed 2015/16 SST over the central tropical Pacific (160°E–150°W, Niño 4 region) only. Exp SC-C is the same as Exp SC-B but for observed SST composite over the central tropical Pacific from historic CP El Niño events that occurred in 1987, 91, 94, 2002, 04, and 09. SSTs in everywhere else are climatology. Each panel depicts precipitation anomalies of "Exp SC-A minus Exp CLIM" (left), "Exp SC-B minus Exp CLIM" (middle), and "Exp SC-C minus Exp CLIM" (right).

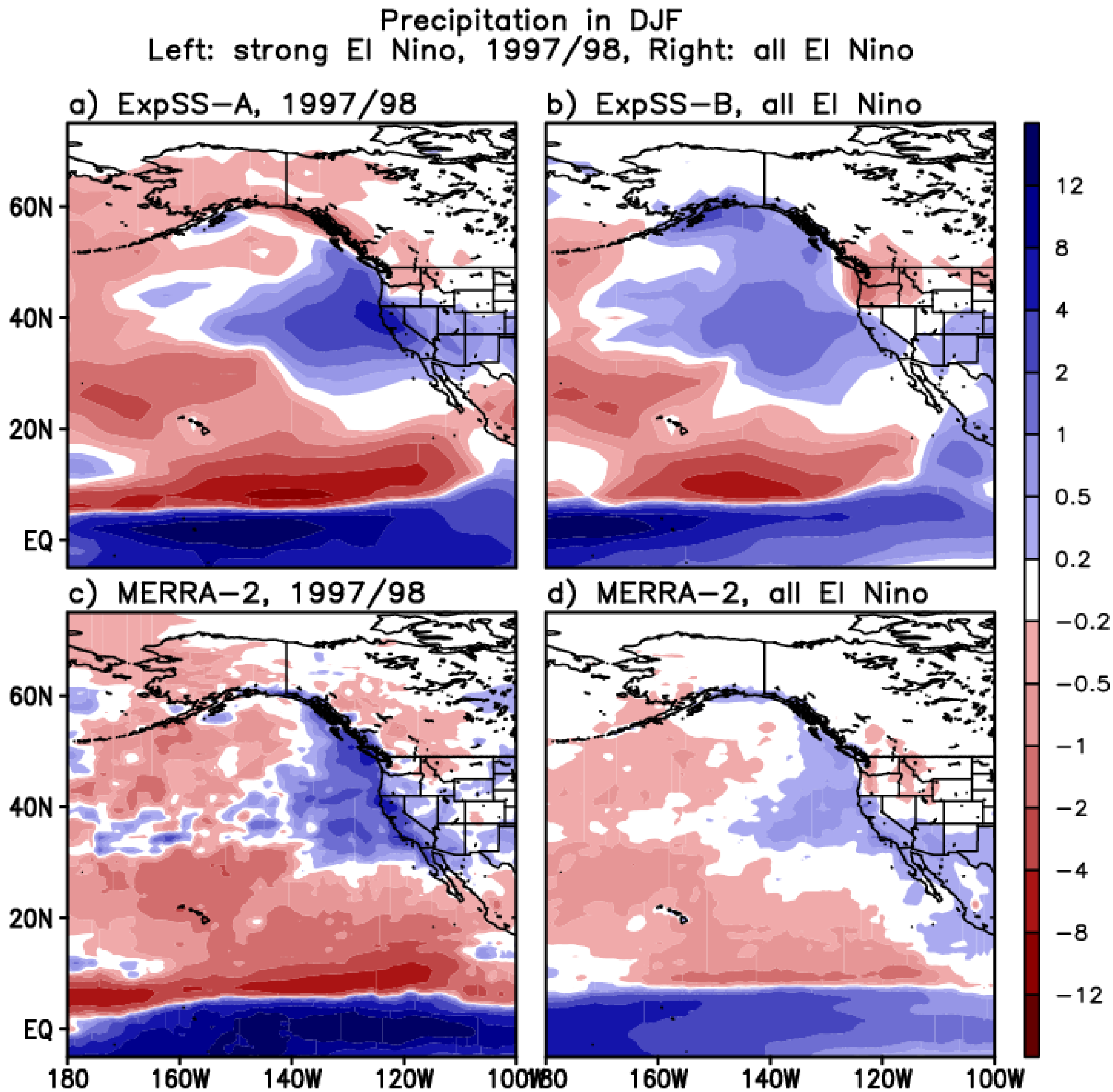

Figure 14. Comparison in DJF precipitation anomalies [mm d^{-1}] between model simulations (upper) (Exp SS, see Section 2.3 and Table 1) and MERRA-2 (lower). The upper-left panel corresponds to the precipitation for a strong 1997/98 El Niño (Exp SS-A), while the upper-right panel is for all historic El Niño composite (1982, 86, 87, 91, 94, 97, 2002, 04, 06, and 09) (Exp SS-B).

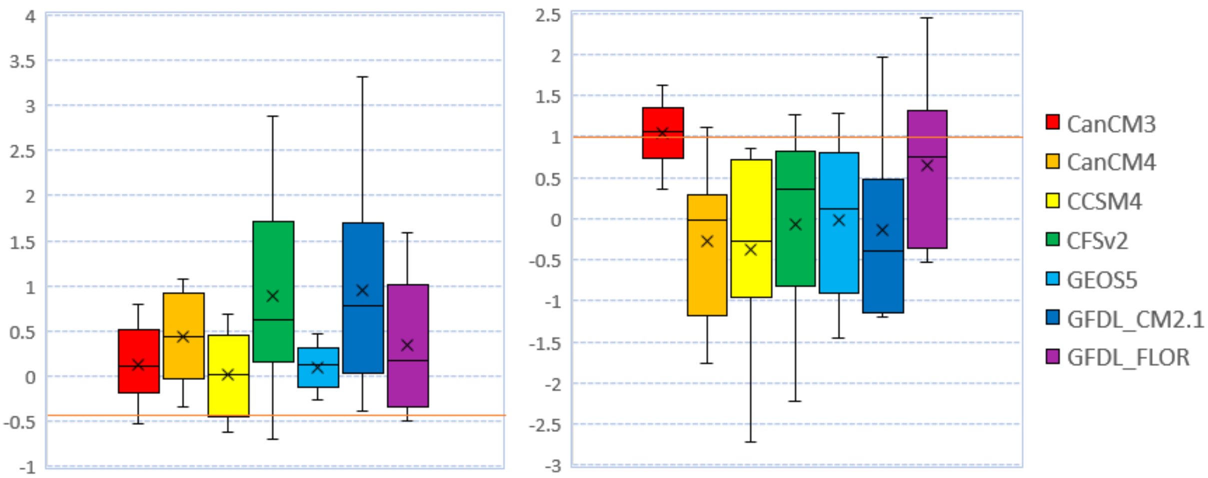

Figure 15. Box-whisker plots of the predicted DJF 2015/16 precipitation anomalies (initialized in November) from the NMME participating models. The left panel is for the precipitation anomaly for the Southern California, Arizona, and Northwestern Mexico (110°–123°W, 25°–37°N) region, while the precipitation on the right panel represents the Northwestern US and Southwestern Canada (120°–130°W, 38°–55°N) region. Horizontal lines in the boxes denote the 1st quartile (bottom edge), median (inside boxes), and 3rd quartile (top edge). Crosses inside boxes are the mean, and the whiskers represent spread of model ensemble. Horizontal orange lines are the observed precipitation anomalies.